International Journal of Impact Engineering 193 (2024) 105042

Contents lists available at ScienceDirect

International Journal of Impact Engineering

journal homepage: www.elsevier.com/locate/ijimpeng

Experimental and virtual testing of mode II and mixed mode crack propagation under dynamic loading

José M. Guerrero [a,*], Emilio V. González [a], José A. Artero [b], Adrián Cimadevilla [b], J.M. Rodríguez-Sereno [b], Joan A. Mayugo [a], Elisabeth De Blanpre [c], Vincent Jacques [c]

[a] AMADE, Polytechnic School, Universitat de Girona, Campus Montilivi s/n, E-17003 Girona, Spain
[b] Department of Continuum Mechanics and Structural Analysis, University Carlos III of Madrid, Avda. de la Universidad, 30, 28911 Leganés, Madrid, Spain
[c] Dassault Aviation, 75008 Paris, France

ARTICLE INFO

Keywords:
Strain rates
Testing
Dynamic loading
Split Hopkinson bar
Composite laminates
Finite element method
Fracture toughness

ABSTRACT

Under static loading, measuring experimentally the mode II and mixed mode fracture toughness of composite materials and adhesive joints is well standardised. However, under dynamic loading, no standard procedure has been defined yet. Therefore, this paper proposes an experimental methodology to measure the mode II and mixed mode interlaminar fracture toughness of composite materials and adhesive joints. The methodology is based on a modified split Hopkinson compression bar. Two different data reduction schemes are explored and compared, one based on measuring the crack length, and another based on measuring the force from the strains in the transmitted bar. The two data reduction methods provided considerably different results. By using the method based on measuring the force, the mode II and mixed mode fracture toughness for both interlaminar and adhesive joints decreased for higher strain rates, while the opposite was found with the other approach. The method based on the crack length measurement was deemed to be unreliable due to the difficulties in measuring it.

1. Introduction

Carbon Fibre Reinforced Polymers (CFRP) are widely employed in lightweight applications, such as in aerospace, thanks to the excellent stiffness and strength to weight ratio they offer [1–5]. Nonetheless, their heterogeneity and quasi-brittle failure behaviour and the lack of knowledge for complex loading conditions and environments, often leads to a large number of experimental testing campaigns and reliable numerical analysis to certify composite structures. Consequently, reliable numerical tools and experimental methodologies are essential for an accurate design [3]. Under quasi-static loading, and even under fatigue, experimental testing is well standardised. Similarly, several numerical models have been developed with relatively good predictive capabilities [6–10]. However, under dynamic loading, no standard procedure has been defined yet. In addition, there is a lack of models with predictive capabilities under dynamic loading.

Composite materials are commonly subjected to dynamic loading, such as impact scenarios in an aircraft (*e.g.* tool drop, debris impact, hail or bird strike) [2,3,11,12]. These impact events can cause complicated damage processes, like fibre breakage, matrix cracking, delamination or fibre–matrix debonding. Among this, delamination, which consists in the debonding of two plies, is a particular concern since it may lead to significant stiffness loss and subsequent catastrophic failure of the structure. In line with this, adhesive joints are widely used in composite structures thanks to the fact that, unlike bolted joints, they avoid the need to introduce holes causing stress concentration and there is a potential weight saving by reducing the number of parts [13]. The strength and fracture toughness of these joints also need to be well characterised, such as under different conditions including high strain rates, in order to avoid catastrophic separation of the joint [3,14,15].

Since polymers are known to suffer from strain rate effects, *i.e.*, their response is dependent on the loading rate [3,14,15], it can be expected that the matrix dominated properties of composite materials, such as the in-plane shear strength or the interlaminar fracture toughness, also depend on the strain rate [3,14,16,17]. Likewise, due to the polymer nature of adhesives, adhesive joints may also exhibit strain rate dependent properties [14,15].

Several investigations have been carried out to understand the influence the strain rate has on the interlaminar fracture toughness of composites and adhesive joints in mode I, mode II and mixed-mode [5,13–15,18–39]. Typically, tests have been carried out using

* Corresponding author.
E-mail address: josemanuel.guerrero@udg.edu (J.M. Guerrero).

https://doi.org/10.1016/j.ijimpeng.2024.105042
Received 22 December 2023; Received in revised form 8 April 2024; Accepted 29 June 2024
Available online 3 July 2024
0734-743X/© 2024 The Author(s). Published by Elsevier Ltd. This is an open access article under the CC BY-NC license (http://creativecommons.org/licenses/by-nc/4.0/).

either adapted hydraulic testing machines [21,38,39], drop tower [40], or the classical Split Hopkinson Pressure Bar (SHPB) [3,5,15]. In mode I loading, wedge Double Cantilever Beam (DCB) specimens have been generally used, while in mode II, the End-Notched Flexure (ENF) specimen geometry has been employed due to its simplicity. Under mixed-mode, the Single-Leg Beam (SLB) has been considered [15] due to its similarity with the ENF specimen. Other less classical specimen configurations have also been proposed, such as the transverse crack tension specimen for mode II [3]. Despite all work, there is still no consensus regarding the strain rate influence on the material properties [3,5,15].

Maikuma et al. [19] investigated the dynamic mode II interlaminar fracture toughness of unidirectional graphite/epoxy and graphite/polyetheretherketone composites, using the centre notch flexural specimen. The tests were carried out with a falling weight impact tester. The dynamic fracture toughness was found to be smaller than the quasi-static. Kusaka et al. [22] presented a modified SHPB for evaluating the dynamic mode II interlaminar fracture toughness of carbon/epoxy laminates. At low strain rates, the fracture toughness was found to increase, but a negative strain rate effect was found for higher loading rates. Oppositely, Tsai et al. [23], using a modified ENF specimen, found no strain rate effect for unidirectional glass/epoxy and carbon/epoxy composites. Later, Wu et al. [26] used the SHPB to determine the dynamic mode I and mode II interlaminar fracture toughness of a unidirectional graphite–fibre/epoxy composite, by testing modified three-point bending and compact shearing specimens. A 10%–20% decrease was found for mode I, but no effect for mode II.

Blackman et al. [13] explored the dynamic mode I fracture toughness of adhesive joints, between unidirectional carbon/epoxy composites and between aluminium adherents. To do so, DCB and tapered DCB tests were carried out in a servo-hydraulic testing machine. The mode I dynamic fracture energy was around 40% lower than the quasi-static. Colin de Verdiere et al. [29] used a modified end loaded split apparatus, mounted on a drop weight impact tower, to obtain the mode II interlaminar fracture toughness of carbon non-crimp fabric epoxy composites. A positive strain rate effect was found. Opposite to this, Wiegand et al. [31] found no strain rate dependency with ENF specimens tested in a SHPB.

Later, Isakov et al. [37] developed a wedge double cantilever beam specimen for obtaining the dynamic interlaminar mode I fracture toughness with a SHPB. No strain rate effect was seen for the tested carbon/epoxy specimens. Lißner et al. [15] investigated the strain rate effect of adhesively bonded titanium specimens under mode I, II and mixed mode, using the SHPB with a data reduction method fully based on Digital Image Correlation (DIC). The results showed a decrease of fracture toughness with the strain rate for all modes. Shamchi et al. [5] developed a modified SHPB for testing ENF specimens, including a transmitted bar. They found a marginal increase in the mode II interlaminar fracture toughness with unmodified carbon/epoxy laminates. More recently, Medina et al. [38,39] presented a novel guided double cantilever beam method for testing mode I specimens, under dynamic loading, in a universal testing machine. The results showed no apparent strain rate effect in a unidirectional carbon/epoxy thermoset laminate.

As a summary of the literature review, some authors have found a decrease of toughness with higher strain rates [15,18,19], while others found a marginal increase or even no effect [5,23,26,29,31,33]. The reported discrepancies may arise by the lack of standardised test methods for dynamic loading: different use of specimen configuration, distinct data reduction methods employed and variations in the testing set-up [3,5].

As evidenced, the current literature shows that there is no clear methodology (test set-up, data reduction method, etc.) to measure experimentally the interlaminar strength and fracture toughness of composites and adhesive joints under dynamic loading. Furthermore, the effect the strain rate has on the interlaminar strength and fracture toughness is yet unclear. In view of this, in this work we make use of the SHPB to test, under dynamic conditions, an ENF specimen (for mode II) and an SLB (for mixed mode) crack propagation tests. Two cases are analysed. In the first, we obtain the strength and interlaminar fracture toughness of ENF and SLB specimens of an aeronautical carbon/epoxy composite. Instead, the second case corresponds to a bonded joint between two carbon/epoxy adherents. In all cases the fracture toughness is computed as a function of the strain rate, by making use of two different data reduction methods based on the literature [5,15], and their limitations are discussed. This is a key difference from previous studies, where only one data reduction method was used [5,15]. In addition, a numerical finite element model was developed to design the experimental test set up and verify the test conditions are adequate to break the specimens in the desired manner. The experimental campaign is carried out based on the finite element model, and the predictions obtained to design the tests are then verified. Further, limitations of the approach and perspectives for future research are given. Accordingly, the article is organised as follows: first, we present the numerical model and the experimental test set-up; next, the data reduction method is explained; and finally, the results and conclusions are presented.

2. Materials and methods

This section describes the materials and specimens, the finite element models, the experimental test set up and campaign, and finally, the data reduction methods.

2.1. Specimens

In order to perform the experimental campaign guaranteeing an appropriate crack propagation and correct development of the test, several finite element models were run a priori for designing the experimental campaign. In total, four different cases have been defined:

- ENF (mode II): (a) adhesive joint and (b) interlaminar characterisation.
- SLB (mixed mode): (a) adhesive joint and (b) interlaminar characterisation.

The ENF and SLB specimens are shown in Fig. 1. The specimens are 20 mm width, 100 mm long and the total thickness is 6.144 mm, so that the thickness of each arm is 3.072 mm. The total span length is 90 mm. In the SLB, the bottom arm is shorter in order to accomplish the mixed-mode loading, which is obtained by laying the top arm (instead of the bottom) on the left support. The length of this bottom arm was selected as short as possible, since otherwise during testing, the arm would vibrate causing load oscillations and affecting the results. To guarantee a stable crack propagation, the pre-crack length of the ENF, a_0, is taken as 0.7 times the half span length, leading to $a_0 = 31.5$ mm. On the other hand, the SLB specimen has a pre-crack length of 32.5 mm. With these considerations, the mixed mode ratio is around 42%, see Section 2.4.1 for all related equations.

Several simulations had to be carried out to optimise the specimen dimensions. The final dimensions (width, thickness, length, span length, etc.) were selected to avoid failure of the adherents while guaranteeing crack propagation, maximise the load equilibrium during the test, and be able to measure all necessary test data with the available equipment. For this reason, we note that the dimensions do not correspond with the typical ones in the quasi-static standard [41]. The adhesive and interlaminar specimens are identical. The material of the arms corresponds to the aeronautical CFRP/epoxy thermoset Hexply M21EV/34%/UD200/IMA/150 ATL, with a ply thickness of 0.192 mm leading to a total of 16 plies per arm. The laminate is unidirectional, with the fibres oriented in the length direction. For the bonded specimens, the adhesive corresponds to epoxy FM® 300M adhesive film, .03 PSF, 36 IN.

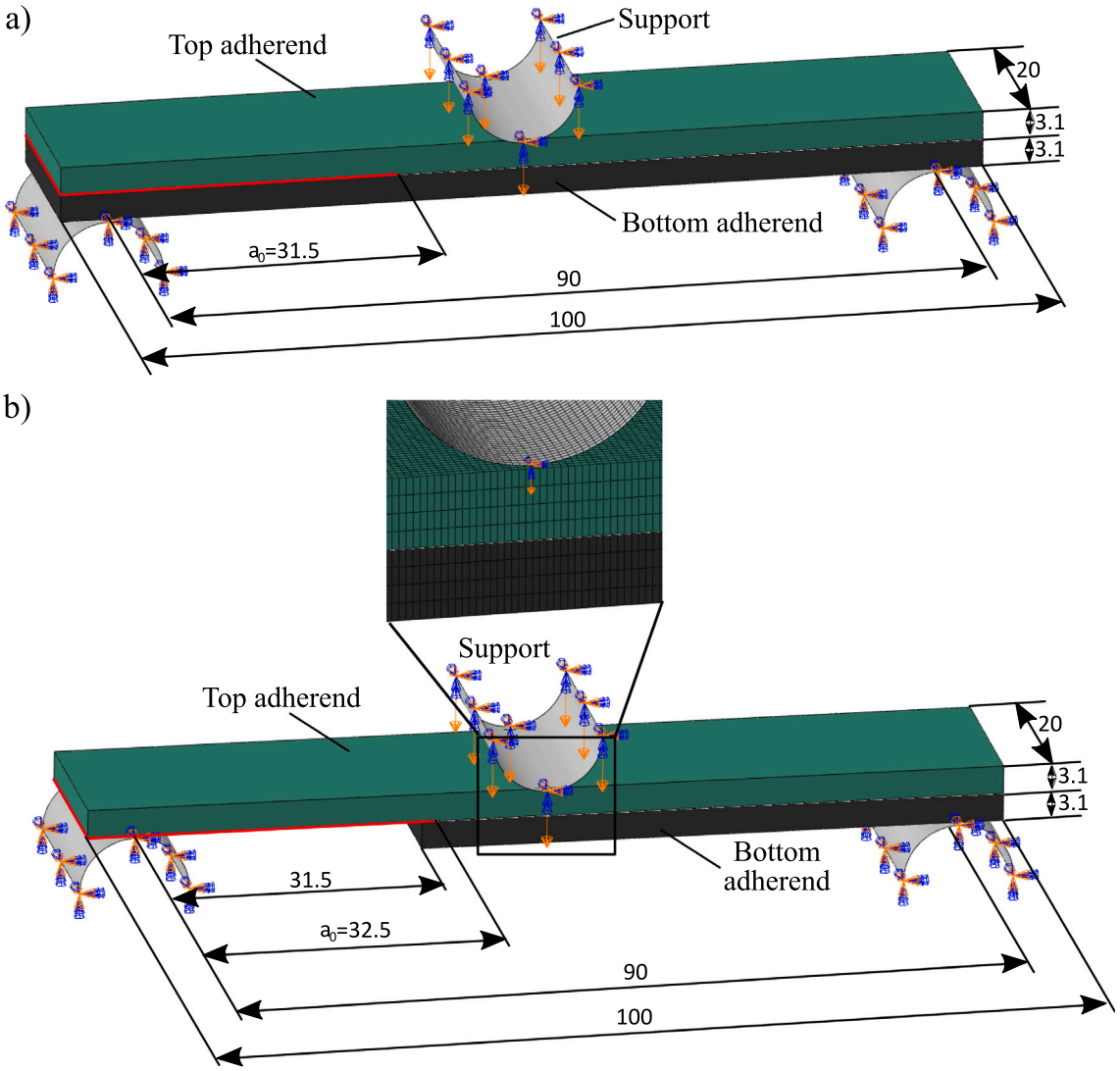

Fig. 1. Designed specimen dimensions and overview of the quasi-static FE model. (a) ENF and (b) SLB. All dimensions are in mm.

2.2. Finite element model

The finite element model was developed in Abaqus 2022, using explicit time integration [42]. While the model attempted to mimic the real experimental test set-up, strain rate effects were omitted. Accounting for strain rate effects requires the use of advanced constitutive models which are not yet available in Abaqus, and are still scarce in the literature [15]. Hence the numerical models were used only to design and validate the experimental test set up, but they do not attempt to reproduce the exact test response.

From a modelling point of view, the only difference between the adhesive and interlaminar specimens is the cohesive properties, while the difference between the SLB and ENF simulations is just the specimen and how it is supported (Fig. 1). Therefore, the numerical methodology is common for all the cases. Both quasi-static and dynamic simulations were performed. These are explained in the upcoming subsections.

2.2.1. Quasi-static model

The quasi-static FE model is based on a typical ENF and SLB quasi-static test. It consists in the specimen (either ENF or SLB) and three roller supports, see Fig. 1. The supports have an end radius of 6 mm, so as to have a reasonable contact area with the specimen. The supports are rigid and modelled by using surface elements of type SFM3D4R (a 4 node surface element with reduced integration [42]). These are especial elements that do not have material properties and do not store internal energy. The specimen arms are modelled as linear elastic, transversally isotropic. Table 1 presents the material properties of the composite. These were obtained experimentally following the appropriate standards [43–45].

Abaqus built-in cohesive surfaces with traction-separation law were used to model the cohesive behaviour and crack propagation during the simulation, both with the adhesive and interlaminar specimens. The damage initiation criteria corresponds to quadratic traction, whereas linear softening is used for damage evolution. Benzeggagh–Kenane interpolation criterion is employed for mixed mode [46]. A penalty stiffness of 100000 was selected for the interlaminar characterisation, which is large enough to not affect the compliance. Instead, for the adhesive, the penalty stiffness was approximated according to the stiffness and thickness of the adhesive. Table 2 presents the cohesive parameters for interlaminar and adhesive specimens. All properties were obtained experimentally in the AMADE lab facilities (expect for the penalty stiffness) by performing quasi-static DCB mode I tests, Calibrated-End Loaded Split (C-ELS) mode II tests and Mixed Mode Bending (MMB) tests for different mixed mode ratios, following the appropriate test standards [47–50]. It is worth noting that two values for G_{II} (and subsequent η) were determined for the interlaminar case. The value of G_{II} = 1.738 N/mm was obtained from the C-ELS tests, in this case η = 1.57 to properly fit the fracture toughness obtained for

Table 1
Engineering constants of the carbon/epoxy composite.

E_{11} (MPa)	$E_{22} = E_{33}$ (MPa)	$\nu_{12} = \nu_{13}$	ν_{23}	$G_{12} = G_{13}$ (MPa)	$G_{23} = E_{22}/\left[2\left(1+\nu_{23}\right)\right]$ (MPa)
147700	8760	0.35	0.4814	5070	2956.66

Table 2
Interlaminar and adhesive cohesive properties. The term η corresponds to the Benzeggagh–Kenane exponent. The values in parenthesis correspond to the properties obtained from the ENF quasi-static tests.

Case	K_{I} (MPa/mm)	K_{II} (MPa/mm)	τ_{I} (MPa)	τ_{II} (MPa)	G_{I} (N/mm)	G_{II} (N/mm)	η
Adhesive	9986.32	3473.5	89	47.5	0.76	2.276	2.56
Interlaminar	100000	100000	46	130	0.31	1.738 (or 2.6)	1.57 (or 2.64)

different mixed mode ratios. However, after performing the ENF tests, $G_{\mathrm{II}} = 2.6$ N/mm and $\eta = 2.64$ were obtained. The authors are unsure of this discrepancy between both tests, but this will be further discussed later in Section 3.2.1.

To mesh the specimen, we used 3D solid elements of type C3D8I (a linear hexahedron with full integration and incompatible modes). This element guarantees that the bending of the adherents are well captured, avoiding hourglassing problems that could occur with the reduced integration element. It also includes an advanced formulation to prevent shear locking [42]. The mesh size was selected to maximise the trade-off between the accuracy of the results and the computational time. The length of the mode I Fracture Process Zone (FPZ), which is more restrictive than in mode II, was computed according to the approach in Soto et al. [51]. The in-plane mesh size in the cohesive area was then set equal to this length divided by 2, leading to an approximate element size of 0.3 mm for adhesive and 0.4 mm for interlaminar specimens. In this way, an accurate energy dissipation should be captured. Notice that a larger mesh size was used for the pre-crack area where no cohesive behaviour is acting. The validity of the selected element size was further confirmed with a mesh sensitivity analysis that we performed, where a mesh size 4 times smaller provided the same results as the one selected. Through the thickness of each arm four elements were used. The rollers also had a mesh size of 0.3 mm. Fig. 1b shows the mesh used in the quasi-static models.

Abaqus general contact algorithm was employed to model the contact. The normal behaviour is modelled with hard-contact, and the tangential with penalty friction formulation, with a friction coefficient of 0.2. This value was assumed based on the measurements carried out in Guerrero et al. [52].

To simulate the quasi-static test, a vertical downwards displacement is slowly applied at the centre roller, whereas the other two rollers are clamped, see Fig. 1. The displacement was applied with a smooth step, with an approximate loading speed of 90 mm/s. To decrease computational time, mass scaling was enforced to reach a minimum stable time increment of $1 \cdot 10^{-7}$ s. These conditions are enough to guarantee negligible kinetic energy during the simulation and assume quasi-static loading.

2.2.2. Dynamic SHPB model

The dynamic model reproduces the Split-Hopkinson Pressure Bar under Compression (SHPB-C) available at the University of Carlos III of Madrid (UC3M), which was used in this work to carry out the experimental campaign. The model includes an incident bar, specimen with pre-crack (either an ENF or SLB specimen), supports and a modified transmitted bar, see Fig. 2. Notice that no impactor is included in the model. Instead, as later clarified at the end of this section, the impact is modelled by using appropriate boundary conditions.

The incident bar is 2.6 m long and has a diameter of 22 mm. It is made of steel and modelled as isotropic linear elastic with Young's modulus of 210000 MPa, a Poisson's ratio of 0.3 and density of 7.85 Kg/m^3. The supports have an end radius of 6 mm in order to have a good contact area with the specimen. They are made of Aluminium, with Young's modulus of 73100 MPa and Poisson's ratio of 0.33. The two supports in contact with the right side of the specimen meet at the transmitted bar, forming a V-shaped piece (Fig. 2). This design allows the wave to travel smoothly from the specimen to the transmitted bar, and it is based on the work by Shamchi et al. [5]. The addition of this 'V shape' transmitted bar is crucial, since it allows to obtain the force of the test directly. The transmitted bar has a diameter of 22 mm and it is made of Aluminium. The total length of all the transmitted bar, including up to the contact of the V-shaped support with the specimen, is 1.4 m. It is worth noting that the two supports on the left of the specimen are simply included to make sure the specimen does not separate from the transmitted bar. Moreover, the transmitted bar (including the 'V shape' arms) is made of aluminium rather than steel because, due to the lower stiffness of aluminium, it allows to reach higher strains in the bar for the same applied force, thus resulting in higher strain magnitudes that can be more accurately measured during the real test.

The specimen and crack propagation are modelled with cohesive surfaces as described for the quasi-static model, using the same material parameters. Again, we meshed the specimen with C3D8I elements, while the other parts use 3D solids of type C3D8R (*i.e.*, a linear hexahedron with reduced integration) since these components are not subjected to bending. The same in-plane mesh dimensions used for the quasi-static model were employed to mesh the specimen, although the mesh was further refined in the contact area between the incident bar end radius and specimen. In addition, one element per ply was used to have a better understanding of the stress levels through the thickness and thus, this led to a mesh size of 0.192 mm through the thickness (compared with 0.768 mm used for the quasi-static). The other parts used a coarse mesh size to reduce the computational requirements. Overall, the models had about 1 million of elements. Fig. 2b shows details of the mesh.

Boundary conditions are applied in order to reproduce the real experimental test. In the real test, an impactor hits the incident bar at a certain speed, producing a strain wave that travels along until the transmitted bar. To simplify the modelling, the impact is not accounted for. Instead, a pressure is applied to the initial surface of the incident bar (where the impact would occur), see Fig. 2. Following SHPB-C theory, the maximum pressure is given by

$$P_{\max} = \frac{V_{\mathrm{imp}} \cdot \rho_{\mathrm{imp}}}{2} \sqrt{\frac{E_{\mathrm{imp}}}{\rho_{\mathrm{imp}}}} \tag{1}$$

where V_{imp} is the impact speed, ρ_{imp} and E_{imp} are the density and Young's modulus of the impactor, respectively, which are the same as for the incident bar (steel material).

Over time, the pressure, P, is applied following an amplitude profile similar to the one that would be obtained in a common test using a cooper pulse shaper, see Fig. 3. This profile was found to be optimum to maximise the crack propagation and the load equilibrium during the test. Notice that the maximum value in the amplitude curve is slightly lower than 1 due to the effect of the pulse shaper. This normalised pressure amplitude profile was considered due to the following reason. The incident wave depends on the impact velocity. To avoid defining a different incident pulse (or pressure) for each simulation, a normalised amplitude profile was generated, in order to remove the velocity dependency. Therefore, the pressure over time (P) that is applied in

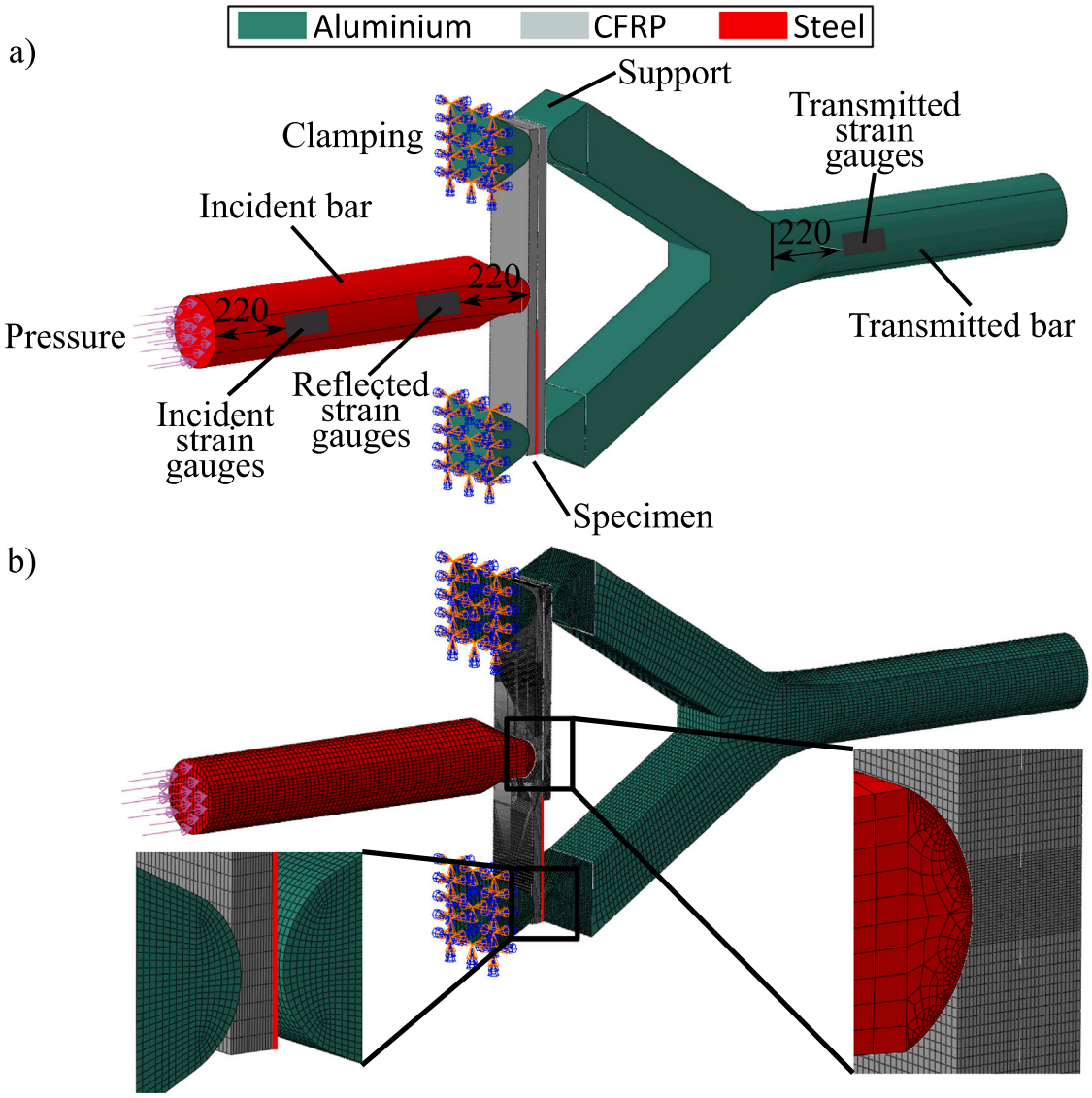

Fig. 2. Dynamic Split-Hopkinson Pressure Bar under Compression (SHPB-C) finite element model. (a) ENF specimen set-up and (b) SLB specimen, showing also details of the mesh. The red line indicates the pre-crack. Dimensions are in mm.

the model is obtained by multiplying the normalised amplitude profile from Fig. 3, with the result of Eq. (1). Consequently, the pressure (*i.e.* incident pulse) that is applied for each simulation is different according to the impact speed, and only the shape and the duration of the incident wave is common for all models. It is worth mentioning that using the real experimental incident wave pulse in the simulations was not possible, since these were carried out before performing the real tests, in order to design the test set up.

Moreover, the two supports to the left of the specimen are clamped, while all the other parts are free to move. Contact between all parts is modelled exactly as in the quasi-static model. The simulation lasts for a total time of 1.3 ms, which is enough to capture the travelling of the wave and its reflection. Once the simulation has finished, the load–displacement curve is extracted from the strains in the transmitted bar, and the crack propagation is verified. The strain gauges in the incident bar are only used to verify the load equilibrium, by comparing them with the strains in the transmitted bar (Fig. 2a indicates the location of all strain gauges). The stresses in the specimen were also analysed to make sure that damage does not occur. Section 2.4 clarifies the actual data reduction used in the simulations and tests.

2.3. Experimental test set up

The experimental test set-ups are based on the FE models described above and are presented in the upcoming subsections for quasi-static and dynamic loading.

2.3.1. Quasi-static test

The quasi-static tests were carried out in the AMADE lab facilities of the University of Girona, following the AITM1-0006 standard. A servo-hydraulic test machine MTS Insight50 with a 50 kN load cell calibrated at 100% was used, including the appropriate test fixture to guarantee the correct boundary conditions for ENF and SLB tests. Lateral marks, separated 1 mm one with another, were created in the specimens to determine the crack length during the test. A Canon camera with a 25x macro was used to accurately monitor the crack propagation, see Fig. 4. The tests were carried out under displacement control with a loading speed of 1 mm/min. In total, a batch of 6 specimens was tested for each case (ENF and SLB, interlaminar and adhesive). Thus, 24 quasi-static tests were done. The data reduction was performed by obtaining the load–displacement from the machine and the crack length from the camera recordings. The displacement was corrected to remove the compliance of the testing equipment. To do so, we carried out a test

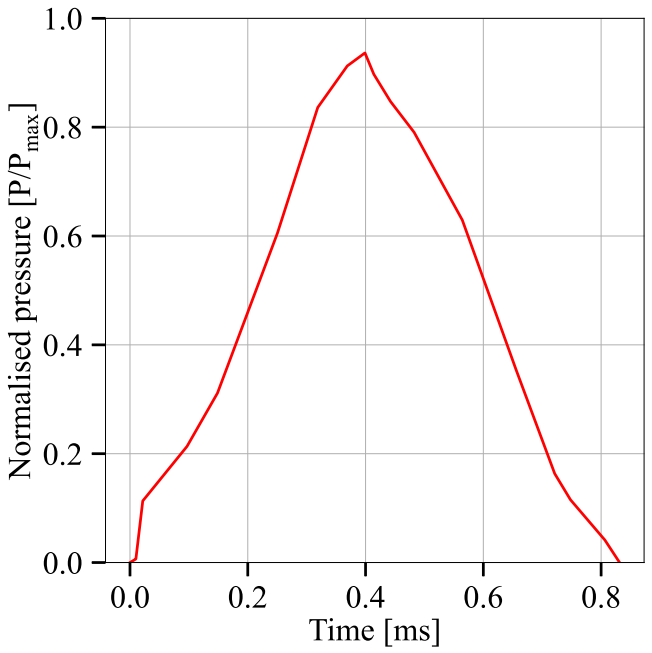

Fig. 3. Normalised pressure profile, P/P_{max}, used to generate the dynamic pulse.

with a very thick steel plate, where the displacement and force were monitored. Since the steel plate is very thick, we can assume that the measured displacement in this test is just the machine displacement. Thus, from this data, we obtained the compliance of the machine and subtracted it from our measurements.

2.3.2. Dynamic SHPB-C test

The dynamic tests were carried out using the SHPB-C available at UC3M. Fig. 5 shows the set-up, which is the same as in the FE simulations. The set-up includes a 1 m long impactor of 22 mm diameter, with the incident and transmitted bars having the same dimensions as in the FE model. The incident bar is instrumented by 2 strain gauge bridges, both bonded at 220 mm from each end side, while the transmitted bar is instrumented with a single strain gauge bridge located 220 mm away from the point where the 'V shape' ends. These gauges are used to perform wave analysis and obtain the force during the test (see Section 2.4). A high speed Photron SA-Z 210-700kfps camera is used to perform DIC, allowing to follow the crack propagation and obtain the displacement of the specimen. The camera uses a Macro 100 mm lens in order to have a detailed image of the central region of the specimen. Shutter speed is set to 1.1 μs and therefore, a proper lighting system has to be used. The image size was set to 256 by 56 pixels, which corresponds to an area of approximately 40×8.75 mm^2. The frame rate was set to 210000 FPS for the mixed mode specimens, while for the ENF it was increased to 700000 FPS due to the fact that these are generally unstable with very rapid crack propagation. Like in the FE simulations, the specimen is simply supported by four supports, where two of them are connected to the transmitted bar by two arms following a smooth 'V shape', see Fig. 5.

The ENF tests were performed approximately at an impact speed of 7.5 m/s, 10 m/s and 13.5 m/s, while the SLB were tested at speeds of 6 m/s, 9 m/s and 12 m/s. A batch of 4 specimens was tested for each impact speed and case (interlaminar or adhesive). Thus, 48 dynamic tests were done in total. Nonetheless, after testing and processing all data, some tests were discarded because there was not a proper contact between the incident bar and the specimen (either before the test or during the test), which invalidated the results. Tables 3 and 4 present the final number of ENF and SLB specimens, respectively, that will be shown with each case and data reduction (see Section 2.4).

It is also worth mentioning that tests were done directly, without propagating the pre-crack in mode I beforehand, as it is generally done in the literature. It was decided not to do so (both in quasi-static and dynamic), since the crack propagation length available in the specimens was already short.

2.4. Data reduction

Due to the lack of standardisation, different data reduction methods have been used for dynamic tests [3]. In this work, two different data reduction methods will be used based on two recent papers [5,15].

On the one hand, Shamchi et al. [5] used strain gauges bonded to the transmitted bar to obtain the force during the test, while the displacement of the specimen (measured at the contact point with the incident bar) was obtained using high speed cameras. From the load–displacement curve, the fracture toughness can be derived using beam theory. The downside of this method is that some signal filtering may be required on the strain gauge measurements to obtain an accurate load–displacement response [15]. In addition, it must be ensured that the inertial effects are small or negligible so as to not affect the force readings.

On the other hand, Lißner et al. [15] used DIC to track both the displacement of the specimen and the crack length during the tests. With this data, and using beam theory, the load–displacement response can be fully derived and from this, the fracture toughness. The advantage of this approach is that strain gauges are unneeded during the test and wave analysis can be avoided. The downside is that measuring accurately the crack length at high rates, especially with an ENF specimen, is quite challenging due to the large instability, i.e high-speed of the crack propagation. Next, we present the two approaches in more detail.

2.4.1. Shamchi et al.: strain gauge method

As advanced before, this method is based on Shamchi et al. [5]. From the strain readings in the transmitted bar, the force of the test can be directly computed with

$$F = \varepsilon_t E_t \pi R_t^2 \tag{2}$$

where ε_t is the strain signal from the gauges in the transmitted bar, E_t is the Young's modulus of the transmitted bar and R_t is the radius.

The displacement, U, is obtained using DIC. To do so, we selected a reference position just at the contact point between incident bar and specimen (see red dot in Fig. 5) and measured the displacement of that point during the test. In order to compute the load–displacement curve, the force and displacement need to be synchronised to the same starting time, since the time the wave reaches the transmitted bar strain gauges is different than the time to reach the displacement measurement position. Therefore, the time for the wave to reach the displacement measurement position was approximated by means of the speed of sound of the bars. By using this reference time the force and displacement are synchronised and the load–displacement response is fully derived.

It is worth mentioning that it is also possible to compute this force from the gauges in the incident bar, but some wave analysis must be done: the reflected signal must be subtracted from the incident signal to obtain the actual force in the test. This is difficult to perform in the experiments and requires significant signal filtering and manual adjustment, making this method quite unreliable. Thus, in this work the force is obtained directly from the transmitted bar in the experiments, since we deemed this to be more reliable, as was also done in Shamchi et al. [5]. Despite this, we will show a comparison of both forces (computed from the transmitted and incident bar) for some simulations and experiments to confirm if the force in the two bars is similar, *i.e.*, there is an acceptable load balance in the test.

After obtaining the load–displacement curve, the fracture toughness can be computed following the Compliance Based Beam Method

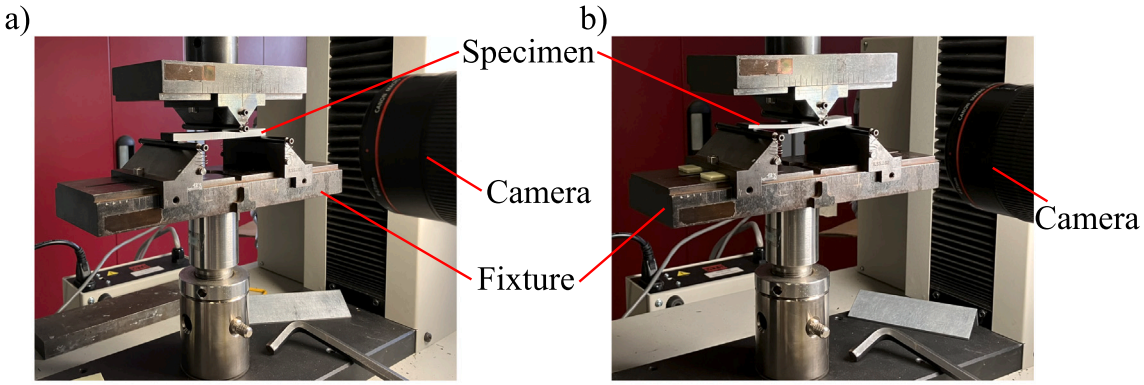

Fig. 4. Quasi-static experimental test set-up. (a) ENF and (b) SLB specimen.

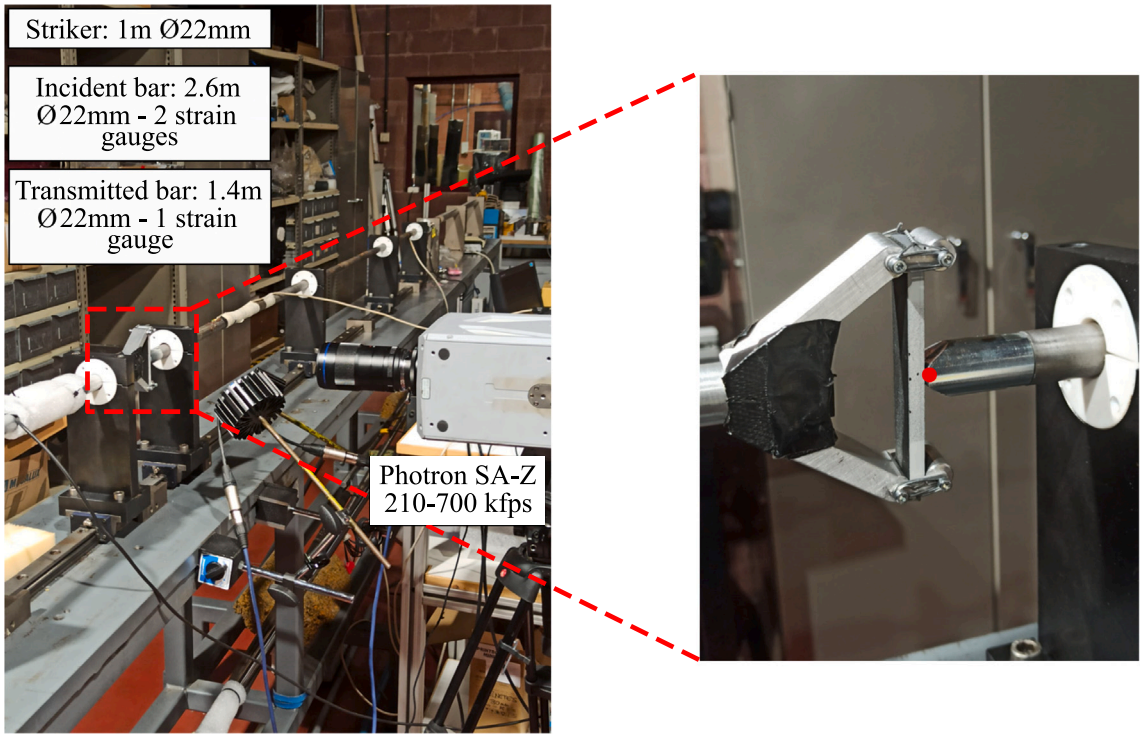

Fig. 5. Dynamic experimental test set-up.

Table 3
Number of ENF specimens shown for each case and data reduction method. Notice that some tests were discarded due to inconsistent results.

Case	Quasi-static	Dynamic V = 7.5 m/s	Dynamic V = 10 m/s	Dynamic V = 13.5 m/s
Adhesive Lißner	6	3	2	4
Adhesive Shamchi	6	3	4	3
Interlaminar Lißner	6	4	3	4
Interlaminar Shamchi	6	4	3	2

Table 4
Number of SLB specimens shown for each case and data reduction method. Notice that some tests were discarded due to inconsistent results.

Case	Quasi-static	Dynamic V = 6 m/s	Dynamic V = 9 m/s	Dynamic V = 12 m/s
Adhesive Lißner	6	4	4	2
Adhesive Shamchi	6	4	3	2
Interlaminar Lißner	6	4	4	4
Interlaminar Shamchi	6	4	4	4

(CBBM) [5,15]. For the ENF specimen (mode II), the equivalent crack method is considered, which includes a correction factor accounting for the FPZ [5,15].

First, the compliance along the test, C, is computed as $C = U/F$, where the displacement, U, and force, F, are known from the experimental measurements. By employing Timoshenko beam theory, the ENF compliance can be related with the crack length, a, with [5,15]

$$C = \frac{U}{F} = \frac{3a^3 + 2L^3}{8bh^3 E_{\mathrm{fII}}} + \frac{3L}{10bhG_{13}} \tag{3}$$

where L is half of the distance between the supports (*i.e.*, the distance from the indenter to one of the supports), b is the specimen width, h is the arm thickness and G_{13} is the Shear's modulus. The flexural modulus, E_{fII}, can be estimated from Eq. (3) with [5,15]

$$E_{\mathrm{fII}} = \frac{3a_0^3 + 2L^3}{8bh^3}\left(C_0 - \frac{3L}{10bhG_{13}}\right)^{-1} \tag{4}$$

where C_0 corresponds to the compliance with the initial crack length, a_0. Then, the equivalent crack length, a_{e}, which accounts for the FPZ, is calculated with [5,15]

$$a_{\mathrm{e}}\left(C_{\mathrm{c}}\right) = \left[\frac{C_{\mathrm{c}}}{C_{0\mathrm{c}}}a_0^3 + \frac{2}{3}\left(\frac{C_{\mathrm{c}}}{C_{0\mathrm{c}}} - 1\right)L^3\right]^{1/3} \tag{5}$$

where C_{c} and $C_{0\mathrm{c}}$ are corrected compliance values, given by

$$C_{\mathrm{c}}\left(C\right) = C - \frac{3L}{10bhG_{13}} \qquad C_{0\mathrm{c}} = C_0 - \frac{3L}{10bhG_{13}} \tag{6}$$

Finally, the fracture toughness of the ENF is obtained with [5,15]

$$G_{\mathrm{II}}\left(a_{\mathrm{e}}, F\right) = \frac{9F^2a_{\mathrm{e}}^2}{16b^2h^3E_{\mathrm{fII}}} \tag{7}$$

On the other hand, for the SLB specimen (mixed mode), the compliance is related with the crack length by [15]

$$C = \frac{U}{F} = \frac{28a^3 + L^3}{32bh^3E_{\mathrm{fm}}} + \frac{3\left(a + L\right)}{20bhG_{13}} \tag{8}$$

The flexural modulus, E_{fm}, can be obtained from Eq. (8) with [15]

$$E_{\mathrm{fm}} = \frac{28a_0^3 + L^3}{32bh^3}\left(C_0 - \frac{3\left(a_0 + L\right)}{20bhG_{13}}\right)^{-1} \tag{9}$$

Therefore, the compliance is obtained as function of the known force and displacement. Then, the crack length, a, is derived during the test from the relationship seen in Eq. (8). With the crack length known, the fracture toughness is then computed with [15]

$$G_{\mathrm{I/II}}\left(a, F\right) = \frac{21F^2a^2}{16b^2h^3E_{\mathrm{fm}}} + \frac{3F^2}{10G_{13}b^2h} \tag{10}$$

The normal and tangential components are given by [15]

$$G_{\mathrm{I}}\left(a, F\right) = \frac{12F^2a^2}{16E_{\mathrm{fm}}b^2h^3} + \frac{3F^2}{10G_{13}b^2h} \qquad G_{\mathrm{II}}\left(a, F\right) = \frac{9F^2a^2}{16E_{\mathrm{fm}}b^2h^3} \tag{11}$$

while the mixed mode ratio can be computed with

$$B = \frac{G_{\mathrm{II}}\left(a, F\right)}{G_{\mathrm{I/II}}\left(a, F\right)} \tag{12}$$

It should be noted that for the SLB the effective crack length (accounting for the FPZ) is not considered [15].

2.4.2. Lißner et al.: DIC method

This method was presented in Lißner et al. [15] and relies fully on the DIC to obtain the load–displacement response. Basically, both the displacement (U) and crack length (a) are monitored during the test. The displacement is measured as in Section 2.4.1, while the crack length is tracked using high speed cameras. Therefore, unlike the method explained in Section 2.4.1, the force is not measured in the tests and wave analysis is not conducted.

Thus, by monitoring the crack length during the test the compliance, C, for the ENF specimen is computed with Eq. (3), while for the SLB (mixed mode test) the compliance is given by Eq. (8). Notice that the flexural modulus is needed to compute the compliance. In this work, the flexure modulus obtained with the method shown in Section 2.4.1 will be used, see Eq. (4) and (9). Alternatively, the longitudinal modulus might be approximated as the flexural modulus. With the compliance and displacement known, the force can be computed directly by $F = U/C$. After this, the fracture toughness for the ENF (mode II) specimen is again calculated using Eqs. (5)–(7). Similarly, for the SLB (mixed mode) case, the fracture toughness is given by Eqs. (10) and (11), where the crack length a is already known from the test measurement. As it can be seen, to compute the compliance (and from that, the force and fracture toughness) it is necessary to measure accurately the crack length and displacement during the test.

3. Results and discussion

This section presents all the results from this research. Firstly, we present a summary of the numerical results that were obtained to validate and design the experimental campaign and then, we present the experimental results.

3.1. Numerical validation of the test design

This section presents the numerical results that were originally obtained to design the experimental campaign. Notice that, for the interlaminar characterisation, the results here shown were obtained with $G_{\mathrm{II}} = 1.738$ N/mm and $\eta = 1.57$ (from previous C-ELS tests; see Section 2.2.1). The objective of these results is to justify the testing methodology, proving it is valid. To do so, the load–displacement behaviour obtained under dynamic conditions was compared with the quasi-static. Since strain rate effects are omitted in the model, the dynamic results should match the quasi-static ones, provided the test is well defined. While the experimental results will be analysed with both data reduction methods presented in Section 2.4, for the sake of conciseness, the numerical validation will be only shown using Shamchi et al. [5] data reduction (Section 2.4.1).

Fig. 6 and Fig. 7 present the load–displacement curves for the ENF and SLB specimens, respectively, under quasi-static and dynamic loading, for different impact speeds. Notice the force is obtained from the transmitted bar, as explained in Section 2.4.1. The analytical solution given by Linear Elastic Fracture Mechanics (LEFM) is also included as a reference.

All curves show the typical response of ENF and SLB tests, with a linear elastic response up to crack propagation. In general, the analytical solution is quite off from the numerical one, especially regarding the stiffness. This is because the LEFM solution assumes beam theory (*i.e.*, the thickness is considered to be very small compared to the length), but in this specimen the thickness is relatively large compared to the length, leading to this difference. In any case, we see that the behaviour during crack propagation are in relative agreement, which validates the model.

The results show that the dynamic curves, for both ENF and SLB, and for adhesive and interlaminar characterisation, are in excellent agreement with the quasi-static one, although with larger oscillations that are normal in dynamic tests. However, even for the largest velocity considered, the response is still in-line with the quasi-static. Consequently, this good agreement confirms that the test set up is well defined and appropriate to perform the real dynamic tests. For the ENF, a velocity of 5 m/s is enough to propagate the crack just a little, while a speed of 15 m/s generates big crack propagation. Instead, for the SLB, a velocity of 2.5 m/s is enough to propagate the crack slightly, while a velocity of 10 m/s generates big crack propagation. Thus, these findings led to the decision of performing the real ENF tests under impact speeds

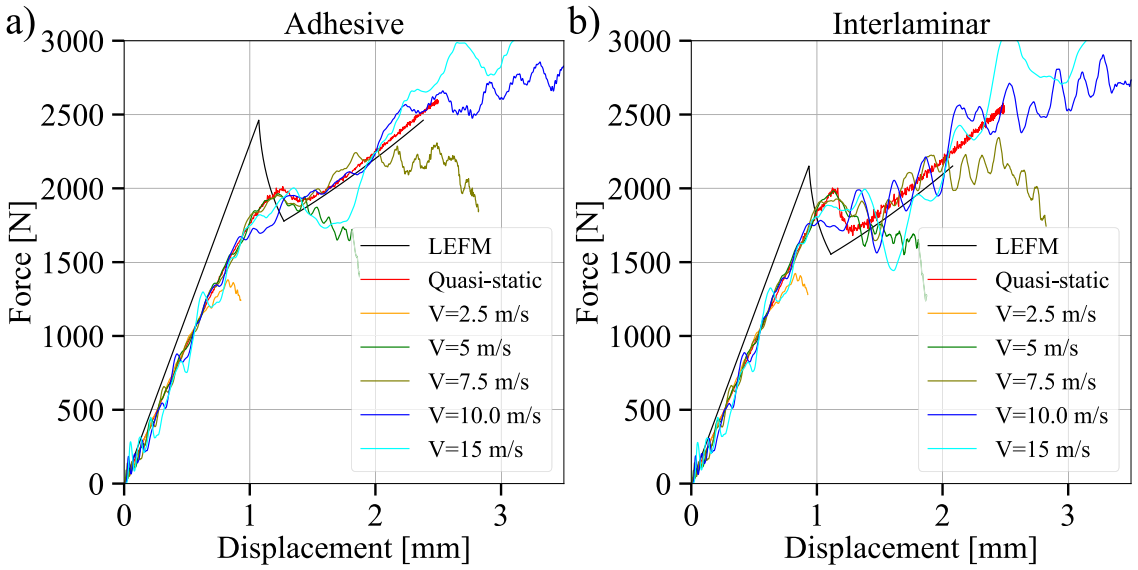

Fig. 6. Numerical load–displacement curves prediction of the ENF (mode II) tests. (a) With adhesive joint and (b) interlaminar characterisation.

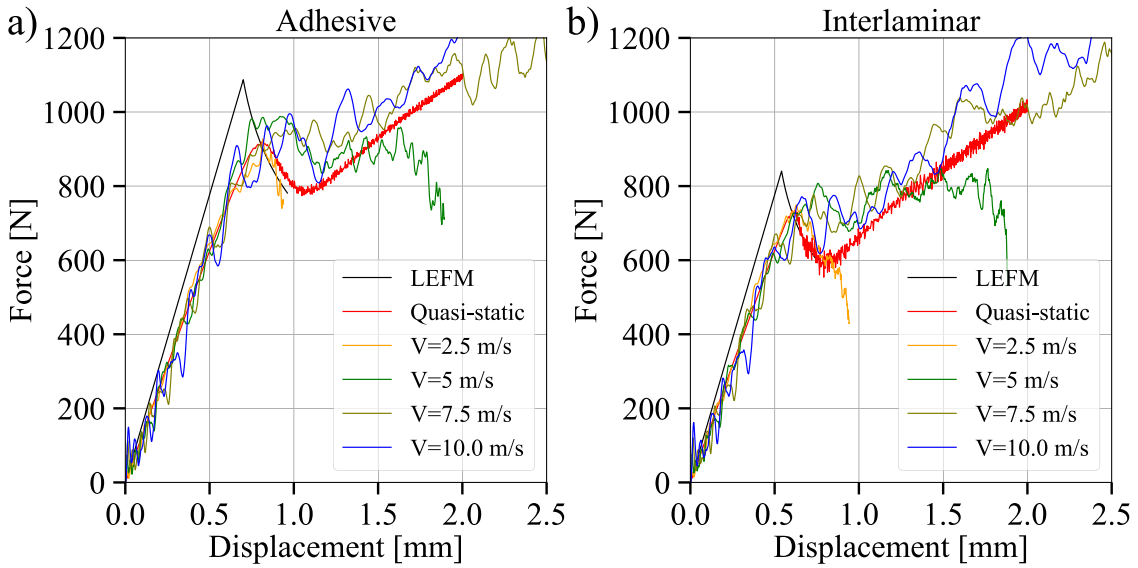

Fig. 7. Numerical load–displacement curves prediction of the SLB (mixed mode) tests. (a) With adhesive joint and (b) interlaminar characterisation.

of 7.5 m/s, 10 m/s and 13.5 m/s, and the SLB under an impact speed of 6 m/s, 9 m/s and 12 m/s.

Further to this, the load balance in the test was checked by comparing the force measured in the transmitted bar with the load in the incident bar, as well as by computing the ratio between the kinetic energy over the internal energy for the specimen. These energies are calculated as the addition of the kinetic and internal energies of each element of the specimen, respectively. These can be obtained in Abaqus by requesting 'ALLKE' and 'ALLIE' energy outputs [42]. This ratio of energies can also give a good indication of the load equilibrium in the test due to the following reason. A good load balance indicates that the applied force in the specimen and the reaction forces (*i.e.*, the load in the incident and transmitted bars) are reasonably equivalent and thus, the inertial loads are not significant. This also implies that the kinetic energy should be small, since the inertial loads are related to this energy. Consequently if the ratio of the kinetic to internal energy is small, a good load balance should be obtained.

Fig. 8 presents the load balance for different velocities of an ENF specimen with adhesive joint. The two forces are in good agreement and show the same trends, especially for an impact speed of 7.5 m/s and 10 m/s. For a speed of 15 m/s the agreement is less good, although the trends between both force signals are the same. Nevertheless, it is important to note that a speed of 15 m/s is reasonably high and thus, it is normal that the load balance is less good for such case. We also note that the incident force shows a lot of oscillations, especially for V = 15 m/s (which commonly occurs for these kind of tests [5]). Filtering this curve would lead to better agreement between the incident and the transmitted forces, however, we preferred to show the raw data. Similarly, the kinetic energy of the specimen is around 20% to 30% of its internal energy when crack propagation onset occurs (around a displacement of 1 mm). This was verified to be the case for the interlaminar specimen as well as the SLB cases. We also note that the stresses were also analysed to verify that no damage will occur in the adherents by simply considering a maximum stress criterion for each material direction.

Overall, the numerical results show that the designed set up is adequate to test the SLB and ENF specimens under dynamic loading using the SHPB-C. Having proved this, next we present and analyse the real experimental results.

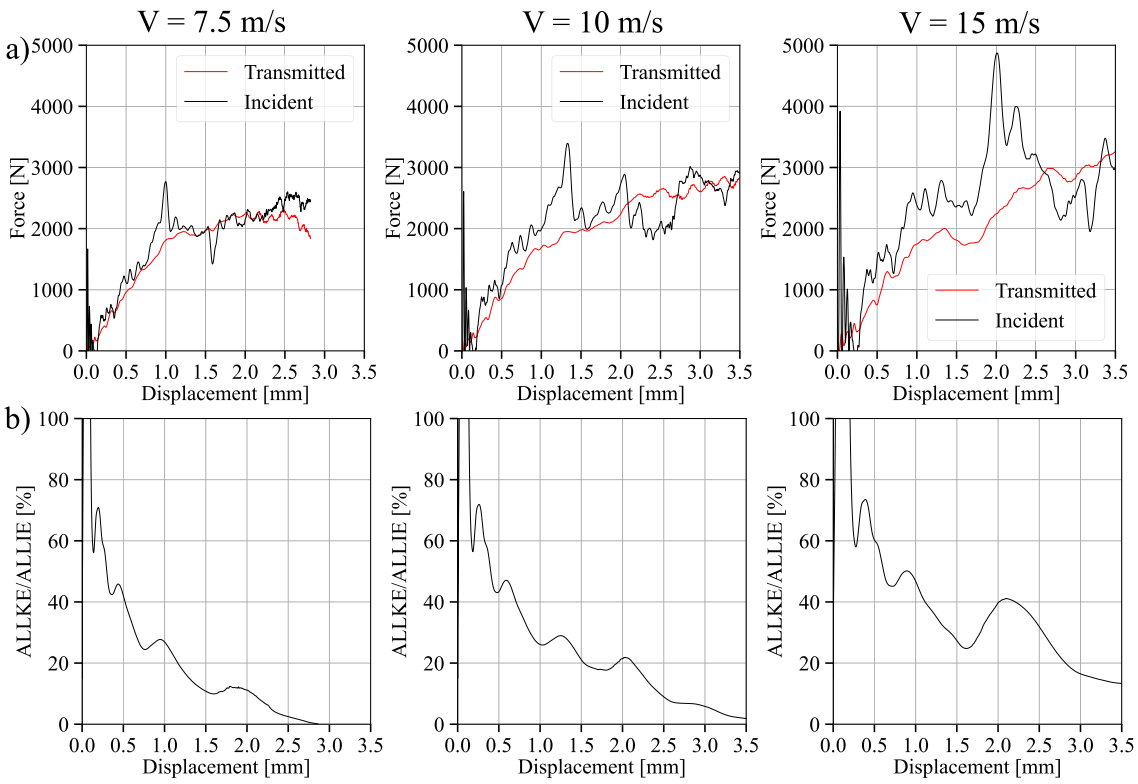

Fig. 8. (a) Numerical comparison of the force in the transmitted and incident bars and (b) ratio of kinetic to internal energy of the specimen. Results are shown for the ENF adhesive joint as a function of the impact speed.

3.2. Experimental results

This section presents the experimental results obtained under quasi-static and dynamic loading. We also include de quasi-static FE predictions as a reference, but this time, the interlaminar models use G_{II} = 2.6 N/mm and η = 2.64 (they correspond to the values obtained in ENF specimens under quasi-static conditions; see Table 2). Dynamic simulations are not shown since the model does not account for strain rate effects and we will focus on the experimental results.

3.2.1. Mode II

Fig. 9 presents the pulse (incident signal), together with the reflection and transmitted signals obtained in one of the ENF adhesive dynamic tests (V = 10 m/s). The incident signal is measured by the strain gauge bridge in the incident bar, located 220 mm away from the impact point (Section 2.3). It is quite smooth, with a continuous rise and a region where the pulse is constant. It was made as long as possible to avoid excessive overlaps in the incident bar. The objective was to reproduce experimentally the same pulse as used in the numerical simulations (since it was found to be optimum), unfortunately, it was impossible to obtain the desired pulse experimentally.

The reflected signal corresponds to the strain measured by the strain gauge bridge in the incident bar located 220 mm to the specimen. Due to the location of the strain gauges that are used to measure this reflected wave, the signal presents an overlap between the incident wave and the 'pure' reflected wave (*i.e.*, the gauges measure the incident pulse when it arrives, but at the same time, the reflection occurs and both signals overlap). For this reason, the start of this curve coincides with the incident signal presenting negative strains, but then it switches to positive strains because it overlaps with the 'pure' reflected wave (Fig. 9). Consequently, the 'reflected' signal is not really the reflected pulse, but rather an overlap between the incident and (real or pure) reflected waves. Therefore, the pure reflected strain is obtained as the reflected minus the incident signals. In this way, the overlap that is experienced is removed and the signal that is obtained is the real reflected wave, that is here referred to as the 'pure reflected wave'. After this, the incident plus the pure reflected signal can be obtained, which should be comparable with the transmitted signal (measured by the strain gauge bridge in the transmitted bar), provided the test is in dynamic equilibrium. In this case, we note the two signals are different indicating the equilibrium was not optimum, but this will be analysed later. In general, the signals were similar for all the tests.

The experimental load–displacement curves obtained, by using the two data reduction methods proposed for the adhesive and interlaminar characterisation, are presented in Fig. 10 and 11, respectively. The quasi-static FE prediction is also included. Notice that, in the data reduction by Shamchi et al. [5], the force is computed in the transmitted bar (and directly from the machine load cell in the quasi-static tests). The results show the expected behaviour, with linear elastic response followed by softening due to crack propagation and stiffening when the crack approaches the half span length. For the adhesive case, crack propagation is smooth and stable, while it is unstable for the interlaminar case, as the large sudden load drop indicates. Overall, the results are quite dependent on the data reduction method as will now be analysed. It is worth mentioning that for the application of the Lißner method, the crack length in the FE models was taken considering that the crack tip was located at the elements with a damage variable equal to 0.5 over 1.0. This threshold was selected since it led to better agreement with the experimental results.

For both adhesive and interlaminar characterisation, the load–displacement curves obtained using the method by Shamchi et al. [5] (*i.e.*, by obtaining the load directly from the test, see Section 2.4.1) provides similar trends: in both cases the onset of propagation occurs earlier with higher impact speeds. Indeed, with V = 7.5 m/s the onset of propagation is in both cases nearly the same as in quasi-static (slightly larger for some specimens, especially for the interlaminar case), and the behaviour is nearly identical to the quasi-static case. However, when the speed is increased to 10 m/s, the load at crack

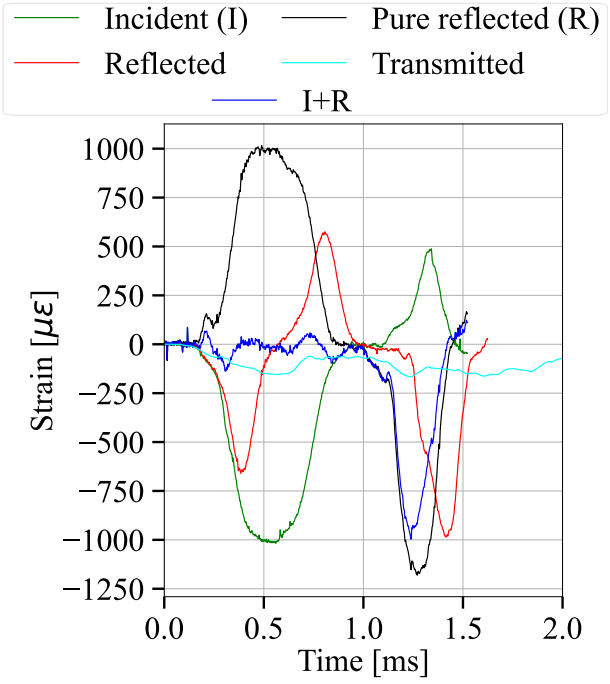

Fig. 9. Experimental incident (I), reflected, pure reflected (R), I+R, and transmitted signals from one ENF adhesive test (V = 10 m/s).

propagation decreases (about 20% and 10% relative to the quasi-static, for the adhesive and interlaminar, respectively) indicating that crack propagation occurs earlier. A further decrease (about 30% and 14%, for the adhesive and interlaminar, respectively, compared with the quasi-static) occurs under a velocity of 13.5 m/s. In general, the curves obtained with this method present some oscillations, particularly for 13.5 m/s, but similarly to the numerical predictions (Section 3.1) the curves are reasonably smooth for these kind of dynamic tests, proving again the validity of the testing set up.

Oppositely, the data reduction method by Lißner et al. [15] leads to completely opposite findings: the propagation onset in dynamic occurs for higher loads than under quasi-static, but the trends are less obvious. For example, for the adhesive, the propagation load onset for 7.5 m/s and 13.5 m/s is about the same, and about 40% higher than the quasi-static; but for 10 m/s it is just approximately 10% higher than the quasi-static. For the interlaminar case, all dynamic results give approximately the same increase in propagation onset force (about 14% on average) regardless of the speed. We also note that the method of Lißner shows less repeatability. In addition, the FE model predicts well the propagation onset force, although the load drop for the interlaminar case is not well captured and thus, the response during crack propagation is not well captured. A potential explanation is that the cohesive law of this material could be not linear (as assumed in the FE model).

Figs. 12 and 13 present the R-curves for the adhesive and interlaminar cases, respectively, whereas Table 5 presents a summary of the average propagation fracture toughness as a function of the speed. Notice that, with the data reduction by Shamchi et al. [5], the first points of the curves were not considered to remove the oscillations for the sake of clarity. This was done by fixing the crack to the initial crack length until crack propagation. A similar approach was conducted by Shamchi et al. [5], where the average flexural modulus obtained from the quasi-static tests was used to perform the dynamic data reduction. Moreover, the average propagation value (Table 5) was computed as the median of all data points from the start of crack propagation until either the crack reached the half span length or it suddenly had a significant change of slope.

In general, the R-curves show the typical response for mode II tests, with an increase of fracture toughness as a function of the crack length, followed by a region where the value approximately stabilises, that is proceeded by an increase again that occurs when the crack approaches the half span length. Results follow the same trends as commented with the load–displacement curves. Hence, the method of Shamchi et al. [5] leads to a significant decrease of fracture toughness with higher speeds. For instance, the adhesive case shows a decrease from about 2.4 N/mm (quasi-static) down to about 0.89 N/mm (for 13.5 m/s), while the interlaminar case decreases from 2.6 N/mm (quasi-static) down to 2.1 N/mm (for 13.5 m/s). Oppositely, the method by Lißner et al. [15] leads to a large increase, with the adhesive case showing an increase from 2.3 N/mm (quasi-static) to between 2.8 N/mm and 4.3 N/mm (depending on the impact speed, largest value is obtained for 7.5 m/s), while the interlaminar increases from 2.3 N/mm to values between 3.1 N/mm to 3.3 N/mm, being larger for 13.5 m/s. Under quasi-static loading though, the two data reduction methods give nearly identical results.

It is interesting to note that the trends here found are the opposite ones observed in Shamchi et al. [5] and Lißner et al. [15]. Lißner et al. [15] found a significant decrease of fracture toughness under high strain rates with ENF adhesive specimens (with metallic adherents and a different adhesive from the one here used), while Shamchi et al. [5] found a marginal increase of the interlaminar fracture toughness under dynamic loading, although the material was again different from the one here used.

The mode II quasi-static interlaminar fracture toughness was found to be 2.6 N/mm, while C-ELS tests carried out before hand with the same material provided a value of 1.7 N/mm, see Section 2.2.1. While the sources for this discrepancy are unclear, the authors have some potential explanations. Firstly, the specimen geometries in both tests were very different; the C-ELS test used standard thin and long coupons, while this was not the case in the ENF test. With the very thick ENF specimens, friction could have played a role as well as the through-the-thickness shear. Secondly, the ENF specimens were tested directly without propagating the crack slightly in mode I beforehand (as it is usually done in order to avoid resin pockets), while this was done with the C-ELS specimens. The presence of a resin pocket in the ENF could have increased the fracture toughness compared with the C-ELS. Thirdly, both C-ELS and ENF tests presented unstable crack propagation, leading to very few propagation data points and thus, the data reduction carried out may be unreliable. In any case, we note that this problem did not occur with the adhesive specimens; in this case, the quasi-static fracture toughness obtained with both tests are equal. The authors will explore this further in future work.

Considering the big difference between the two data reduction methods, the key point is to understand which of the two methods seems to be more reliable. In this regard, the authors believe that the results obtained by the method of Lißner et al. [15] are less convincing due to the following explanation. Under quasi-static loading, crack propagation occurred mostly slow, and still, it was challenging to determine the crack length during the tests for the short and thick ENF and SLB specimens considered. However, for the dynamic tests, the crack propagated very fast, and we faced several difficulties to establish where was the crack, since it was very difficult to detect properly. Fig. 14 shows photos of the crack propagation during one test, showcasing well that the crack tip is difficult to locate. Given that in the data reduction method by Lißner the crack length is to the power of 3, see Eq. (3), small errors in determining the crack length can lead to large errors. On the other hand, the method by Shamchi does not have this issue, since the force is obtained directly from the test and the crack length inversely afterwards. Another advantage by Shamchi approach is that the force includes the oscillations due to the dynamic loading, which can give an idea if the test was too affected by the inertia.

Another important point is that the results with Lißner method show much higher dispersion, again, this could be related to the difficulties

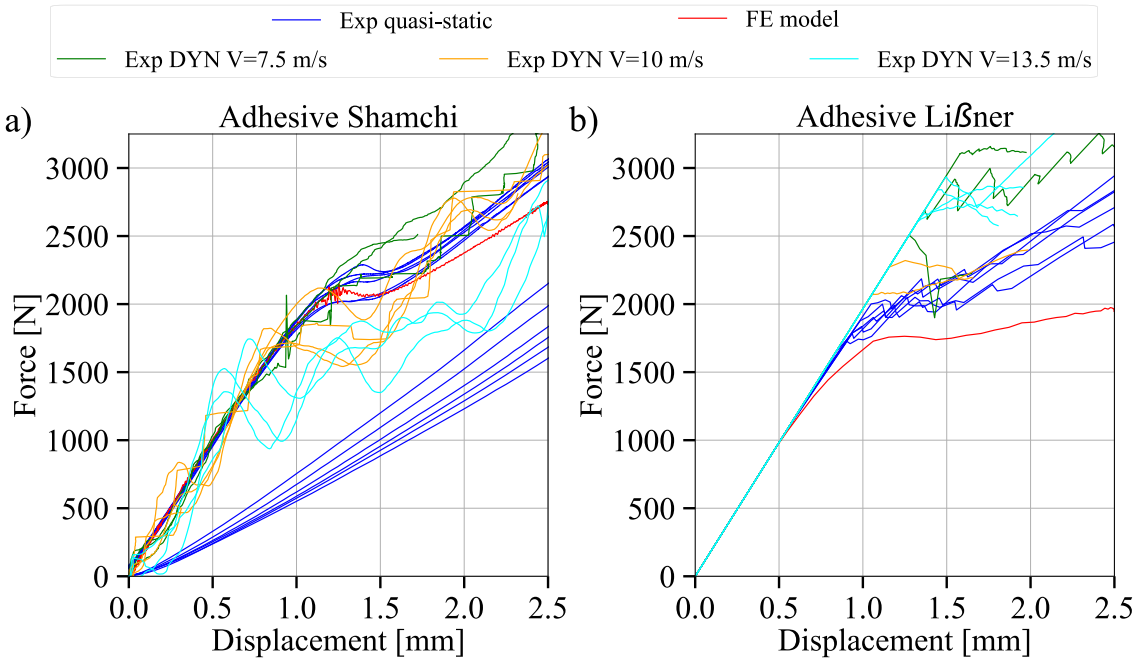

Fig. 10. Experimental load–displacement curves for the ENF adhesive specimens under different impact speeds. (a) With Shamchi et al. [5] and (b) with Lißner et al. [15] data reduction methods, respectively.

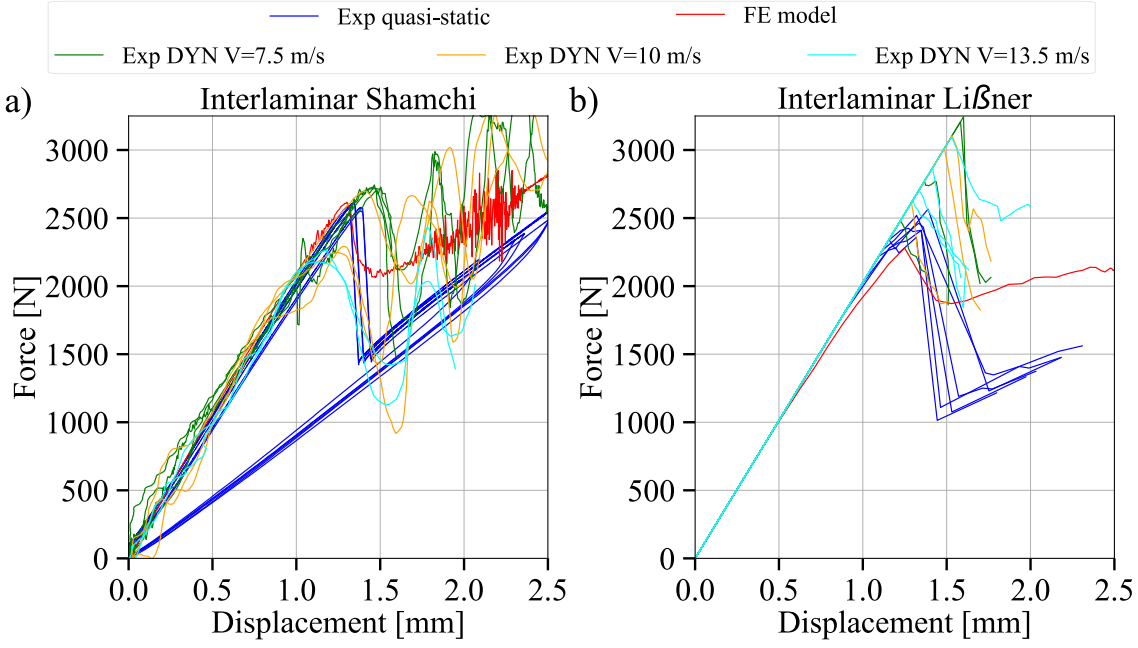

Fig. 11. Experimental load–displacement curves for the ENF interlaminar specimens under different impact speeds. (a) With Shamchi et al. [5] and (b) with Lißner et al. [15] data reduction methods, respectively.

Table 5
Average mode II propagation fracture toughness (in N/mm) as a function of the speed and data reduction method.

Case	Quasi-static	Dynamic V = 7.5 m/s	Dynamic V = 10.0 m/s	Dynamic V = 13.5 m/s
Adhesive Lißner	2.349 ± 0.169	4.320 ± 1.064	2.841 ± 0.320	4.092 ± 0.408
Adhesive Shamchi	2.398 ± 0.295	2.279 ± 0.295	1.773 ± 0.216	0.890 ± 0.178
Interlaminar Lißner	2.317 ± 0.134	3.171 ± 0.476	3.208 ± 0.462	3.348 ± 0.500
Interlaminar Shamchi	2.595 ± 0.057	3.026 ± 0.153	2.360 ± 0.491	2.166 ± 0.037

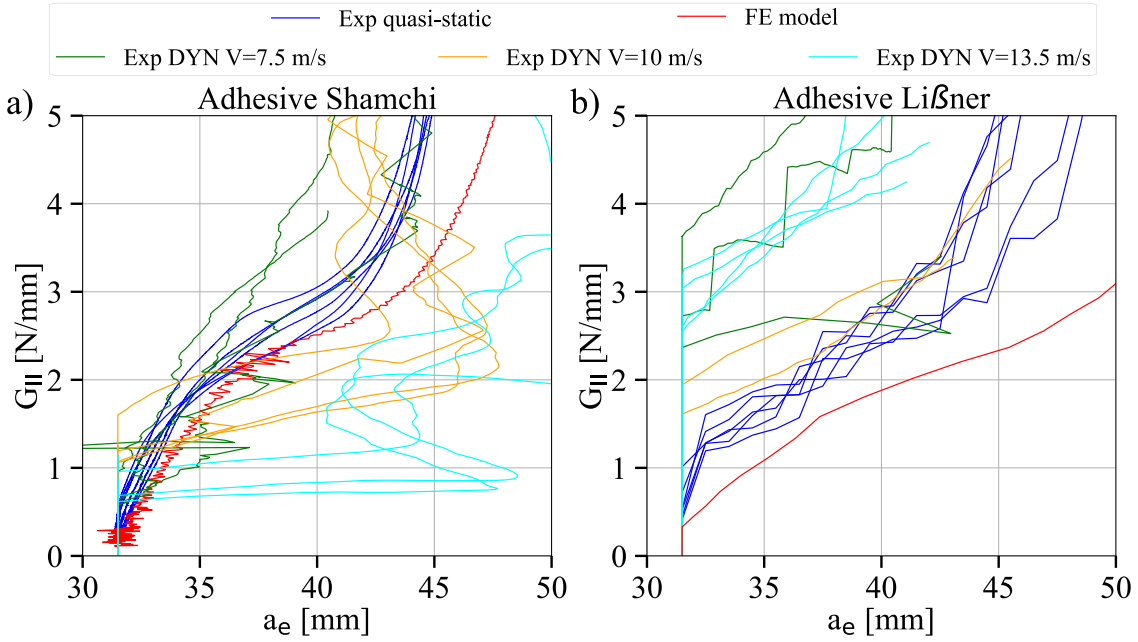

Fig. 12. Experimental R-curves for the ENF adhesive specimens under different impact speeds. (a) With Shamchi et al. [5] and (b) with Lißner et al. [15] data reduction methods, respectively.

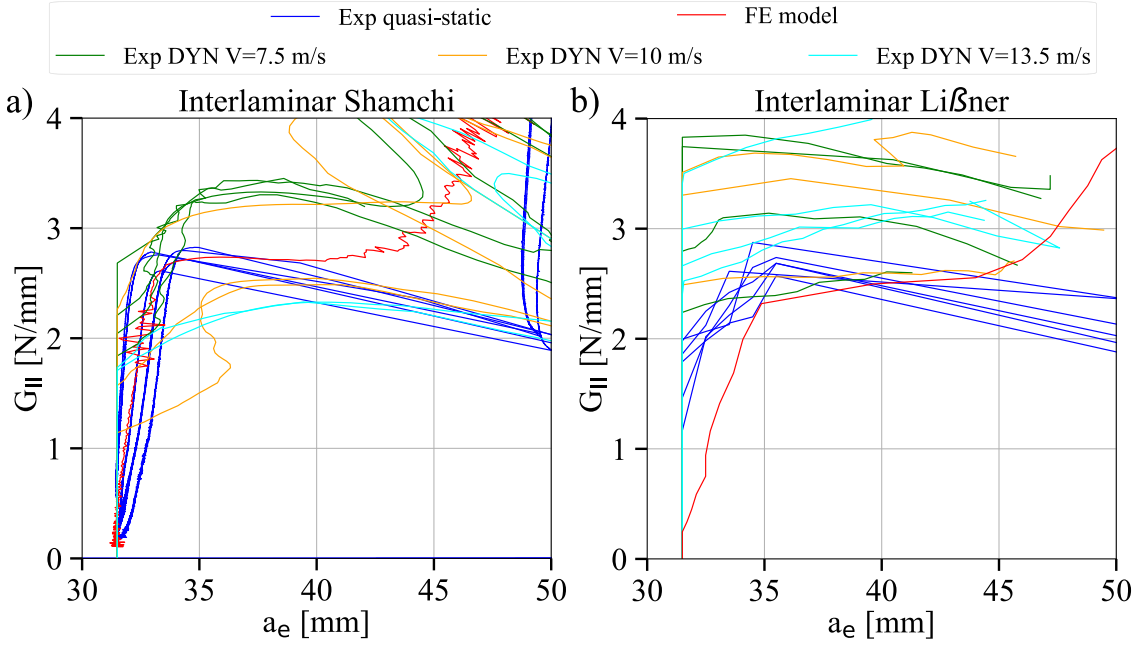

Fig. 13. Experimental R-curves for the ENF interlaminar specimens under different impact speeds. (a) With Shamchi et al. [5] and (b) with Lißner et al. [15] data reduction methods, respectively.

in determining the crack length. Considering all these facts, it seems plausible that the results with Shamchi method are more reliable. These findings show well that the selection of one data reduction method or another is not trivial; results can be heavily biased by this. This can be one of the reasons why there is so much discrepancy of the results in the current literature [3]. A further important point is that the two data reduction methods employed are in reality developed for quasi-static loading. Nonetheless, the relative low oscillations found in the tests justify using them, as done in previous papers [5,15]. In any case, it is also important to remark that in these dynamic tests, there are different sources of error (filtering of the strain readings, synchronisation of the signals, strain gauge precision, perfect and continuous contact between the incident bar and specimens, etc.). Therefore, the results are subjected to uncertainty, which could also explain the difference between both data reduction methods as well as could potentially bias the trends here found. The authors will attempt to explore further these uncertainties in future work.

Fig. 15 shows the load balance during one of the tests for the adhesive case, by comparing the force signal in the incident bar with the force in the transmitted bar. Similar to the simulations, the force in the incident bar presents a heavy amount of noise compared with the force in the transmitted bar, this is a typical issue in this kind of dynamic tests [15]. Nonetheless, the two forces follow similar trends, as analysed next. Both forces show a continuous increase of load until

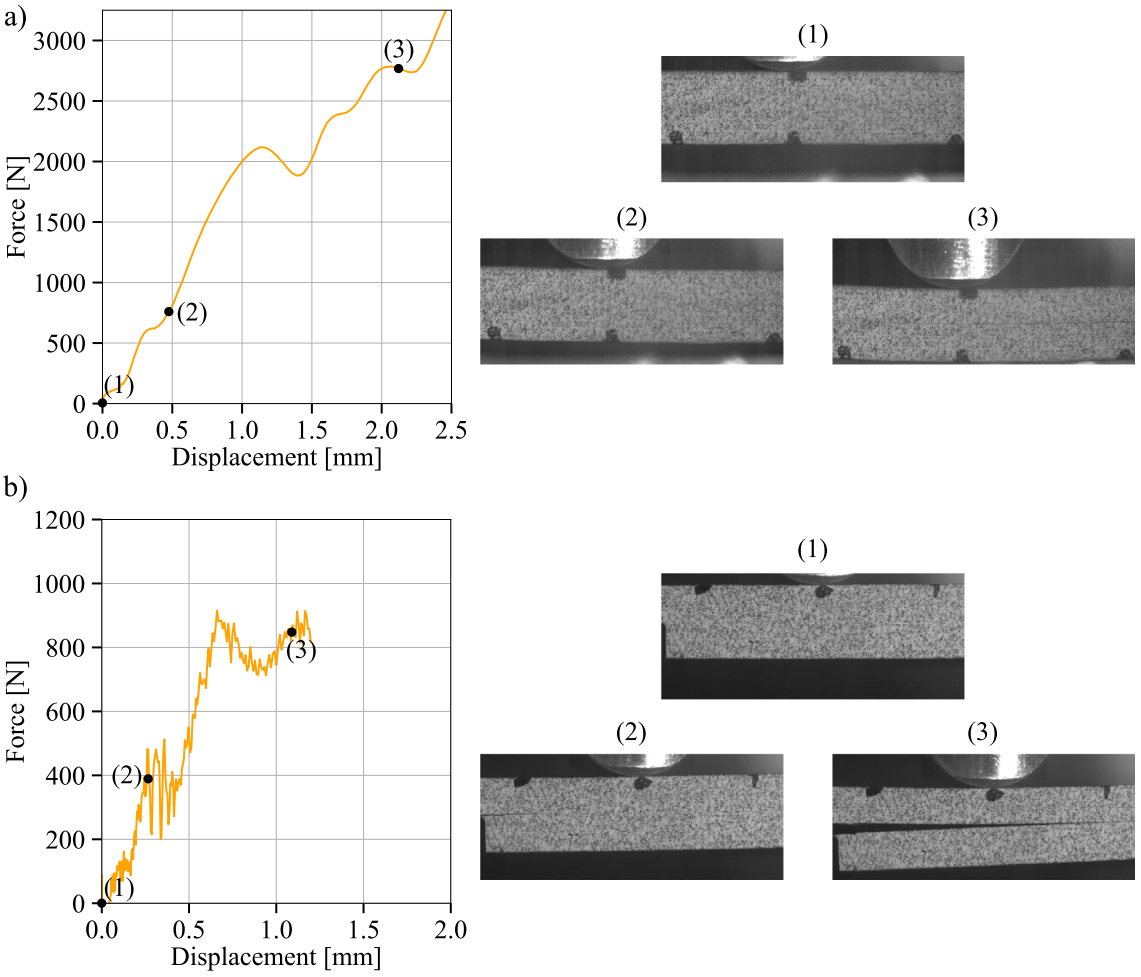

Fig. 14. Photos of the crack propagation during one dynamic test at three different instants. (a) ENF adhesive tested at V = 10 m/s and (b) SLB adhesive impacted at V = 9 m/s.

about 0.5–0.6 ms. After this, both present a decrease of load due to the crack propagation. Between 0.75 and 1 ms the curves show a plateau region (in this regard the incident force has a shorter plateau). Finally, there is a load increase for both cases at around 1.25 ms (although it is much larger for the incident force). Therefore, both curves show similar trends, although it is clear that the load equilibrium is far from ideal, since the absolute force values are different. In this regard, the simulations predicted a much better equilibrium (Fig. 8). It is also worth mentioning that the computation of the incident signal can have large errors, due to the large noise in the signal, in addition to the fact that manual wave analysis is needed to obtain it. Therefore, this result has to be interpreted with care. For this reason, despite the impedance and possible reflections caused by the used transmitted bar with arms, its presence is beneficial since it filters the force, increasing the accuracy of the test rather than taking the force from the incident bar. Unfortunately, this force comparison is not shown in other publications [5,15], which makes it hard to judge further the load balance here found.

In summary, for the adhesive and interlaminar characterisation, we found contradictory trends depending on the data reduction. On the one hand, the inverse method by Shamchi led to an earlier propagation onset and fracture toughness with higher speeds, while with the direct method by Lißner the opposite occurred. The authors believe that it is difficult to confirm whether the results provided by Lißner method are valid or not, as they have the inherent problem of accurately measuring crack propagation at very high speed.

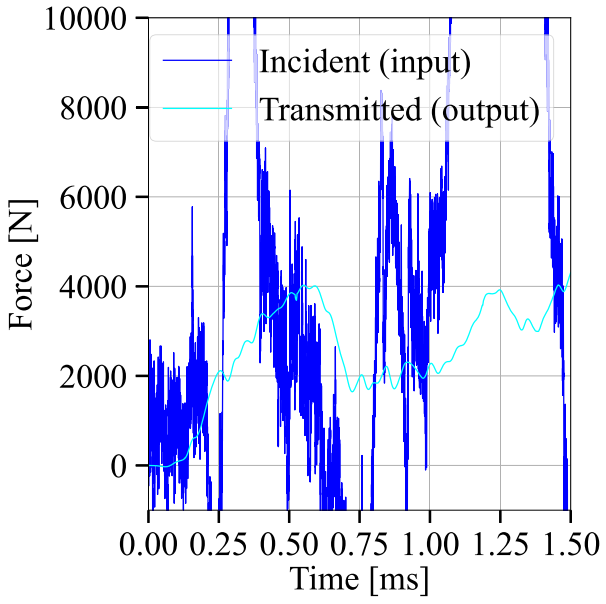

Fig. 15. Experimental measurement of the force in the incident and transmitted bars for one ENF adhesive specimen (V = 10 m/s).

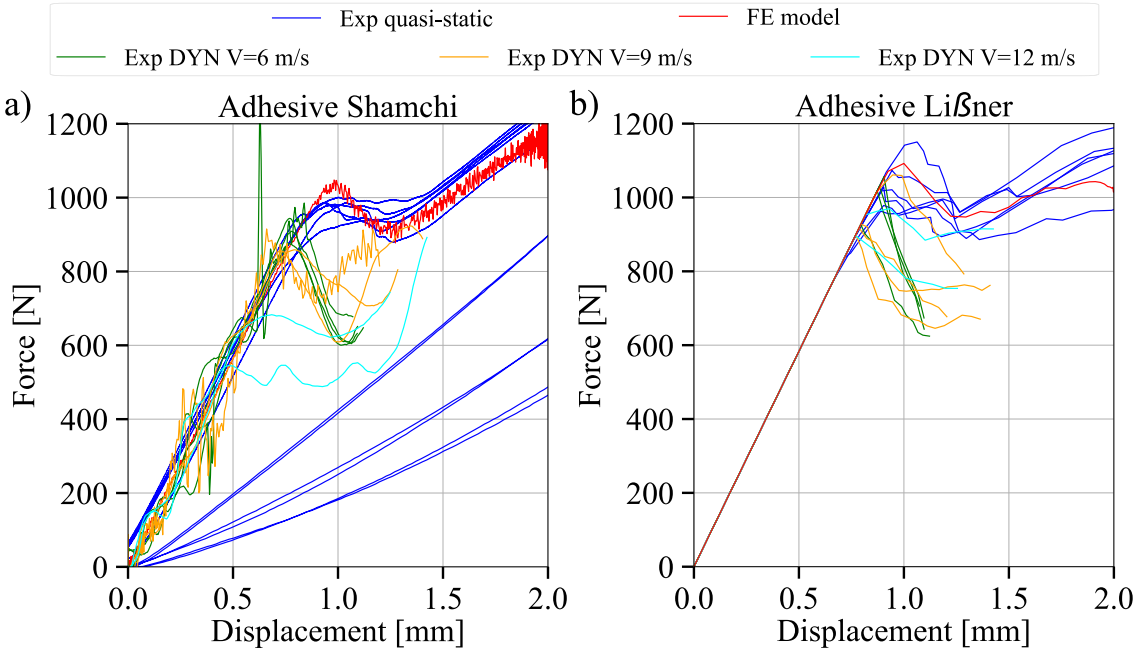

Fig. 16. Experimental load–displacement curves for the SLB adhesive specimens under different impact speeds. (a) With Shamchi et al. [5] and (b) with Lißner et al. [15] data reduction methods, respectively.

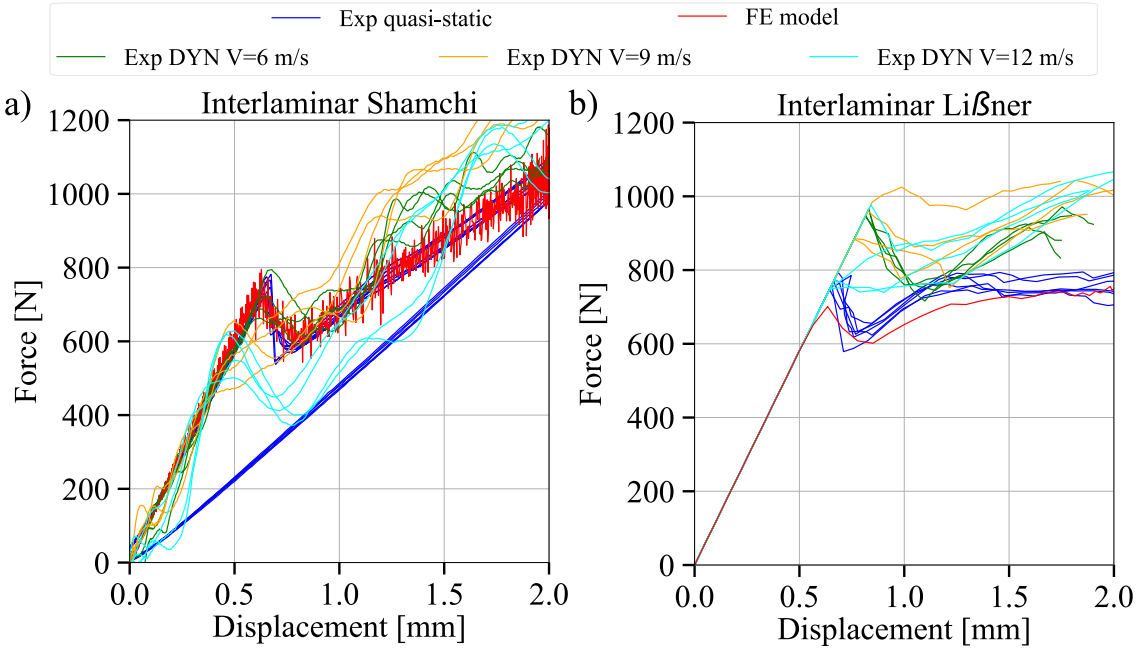

Fig. 17. Experimental load–displacement curves for the SLB interlaminar specimens under different impact speeds. (a) With Shamchi et al. [5] and (b) with Lißner et al. [15] data reduction methods, respectively.

3.2.2. Mixed mode

Figs. 16 and 17 present the load–displacement curves obtained for the mixed mode adhesive and interlaminar cases, respectively, with both data reduction methods. Again, the FE model is also included.

Like the ENF, the curves show the expected response, with a first linear elastic part followed by softening due to the crack propagation, and then hardening when the crack approaches the mid span. The interlaminar case again shows a more unstable response than the adhesive. The numerical model is in reasonable agreement with the quasi-static experiments. In-line with the ENF, for both adhesive and interlaminar specimens, the load–displacement curves obtained using the method by Shamchi et al. [5] shows that the propagation onset occurs earlier with higher speeds. With V = 6 m/s, the propagation onset load of the adhesive case is already 8% lower than the quasi-static, decreasing even further (18%) for 9 m/s and 40% for 12 m/s. For the interlaminar the effect is smaller: with V =6 m/s the propagation onset load is almost the same as the quasi-static, but it decreases around 20% for 9 m/s and by 25% for 12 m/s. All curves presented a reasonable repeatability, with some oscillations but within reasonable limits and being quite smooth. Instead, the results obtained by Lißner et al. [15] data reduction show again some inconsistencies. With the adhesive specimens, the propagation onset load is in general 14% lower in dynamic than in quasi-static, being consistent with Shamchi method. However, there is

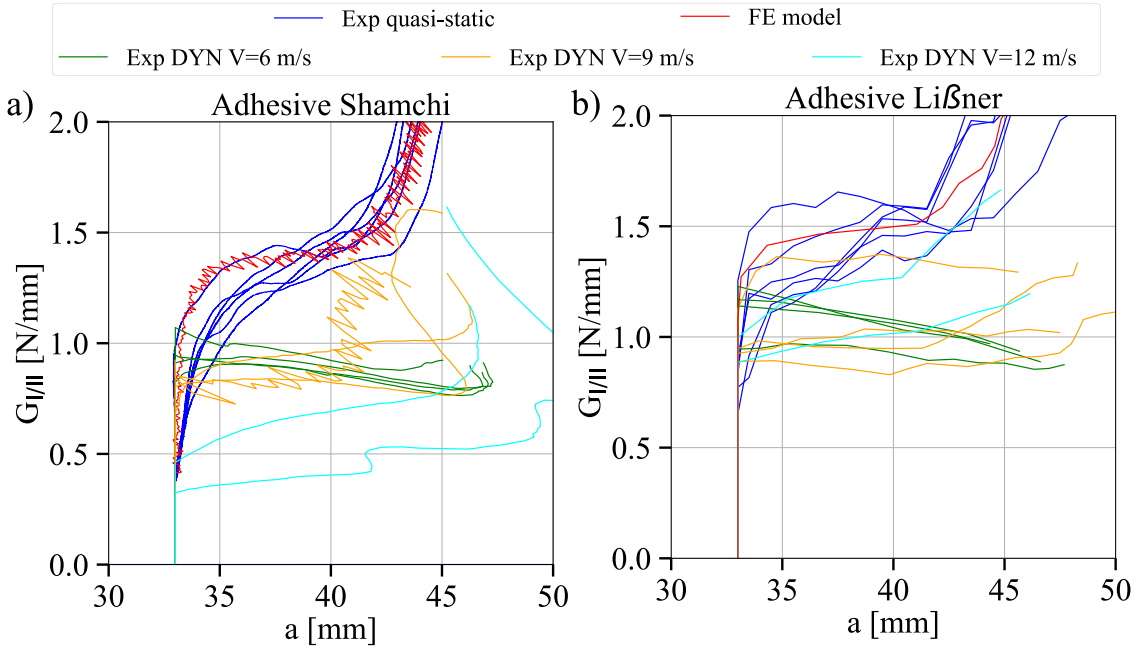

Fig. 18. Experimental R-curves for the SLB adhesive specimens under different impact speeds. (a) With Shamchi et al. [5] and (b) with Lißner et al. [15] data reduction methods, respectively.

Table 6
Average mixed mode propagation fracture toughness (in N/mm) as a function of the speed and data reduction method.

Case	Quasi-static	Dynamic V = 6 m/s	Dynamic V = 9 m/s	Dynamic V = 12 m/s
Adhesive Lißner	1.384 ± 0.109	1.029 ± 0.061	1.047 ± 0.175	1.180 ± 0.164
Adhesive Shamchi	1.164 ± 0.116	0.895 ± 0.021	0.865 ± 0.056	0.538 ± 0.131
Interlaminar Lißner	0.660 ± 0.043	1.019 ± 0.006	1.168 ± 0.164	1.057 ± 0.188
Interlaminar Shamchi	0.593 ± 0.017	0.624 ± 0.065	0.506 ± 0.069	0.387 ± 0.029

not a clear trend, since on average all dynamic specimens give similar propagation onset force regardless of the speed. For the interlaminar case, the results by Lißner method show an average 16% delay of the propagation onset, being in disagreement with Shamchi method. Again, a clear trend is difficult to be established. Overall, these results indicate that under mixed mode loading, the strain rate effects are as important as under mode II, and there is more effect for the adhesive than the interlaminar specimens, at least for the materials analysed here.

Figs. 18 and 19 present the R-curves for the SLB adhesive and interlaminar cases, respectively, while Table 6 presents a summary of the average mixed mode propagation fracture toughness as a function of the speed. The curves show the same behaviour commented with the ENF, with an increase of fracture toughness as a function of the crack length, followed by a region where it stabilises, that is proceeded by an increase again that occurs when the crack approaches the half span length. Results are well in-line with the observations done with the load–displacement curves. For the adhesive specimens both methods show a significant decrease of fracture toughness under dynamic loading: from 1.1 N/mm (quasi-static) down to about 0.5 N/mm (V = 12 m/s) and from 1.4 N/mm (quasi-static) down to 1.1 N/mm (V = 12 m/s) with Shmachi and Lißner methods, respectively. For the interlaminar case, the fracture toughness with Shamchi method decreases from 0.59 N/mm (quasi-static) to 0.38 N/mm (for V = 12 m/s), while with the method by Lißner, it increases from 0.66 N/mm (quasi-static) up to a value between 1.02 N/mm and 1.17 N/mm, without following a clear trend with the impact speed. As it was commented with the ENF (Section 3.2.1), the results obtained with Lißner may be less convincing due to the large uncertainties in the measurement of the crack length, see Fig. 14b. It is also interesting to note that Lißner et al. [15] found a significant decrease of mixed mode fracture toughness with metallic adherents and a different adhesive from the one used here.

In summary, the adhesive case showed a decrease of fracture toughness and earlier propagation onset under dynamic loading compared with the quasi-static, by using both data reduction methods. For the interlaminar specimens, the method by Shamchi led to a decrease of fracture toughness and earlier propagation onset with higher impact speeds, while the opposite trend occurred with the method by Lißner.

4. Conclusions

In this paper, the SHPB-C was employed to characterise experimentally the interlaminar fracture toughness of composite materials and adhesive joints in mode II and mixed-mode under dynamic loading. To do so, FE simulations were carried out to design the experimental campaign. For mode II, ENF specimens were employed while SLB specimens were used for mixed mode. To guarantee the correct boundary conditions during the test (*i.e.* 3 point bending), a modified transmitted bar was designed, which includes two arms forming a 'V shape', where the specimen is simply supported. Two different data reduction methods were used and compared.

The numerical results show that the designed test set-up is adequate to perform the dynamic tests, exhibiting reasonably good force balance during the entire crack propagation despite of the presence of the adapted transmitted bar with the 'V shape' connection. The numerical model, using the commercial features available in Abaqus, was able to reproduce reasonably the quasi-static experiments.

In general, the experimental results under dynamic loading showed different fracture toughness compared to the quasi-static values. Nonetheless, the results were extremely dependent on the data reduction method, leading to significant uncertainty in the computation and interpretation of the data. By using the inverse method of Shamchi,

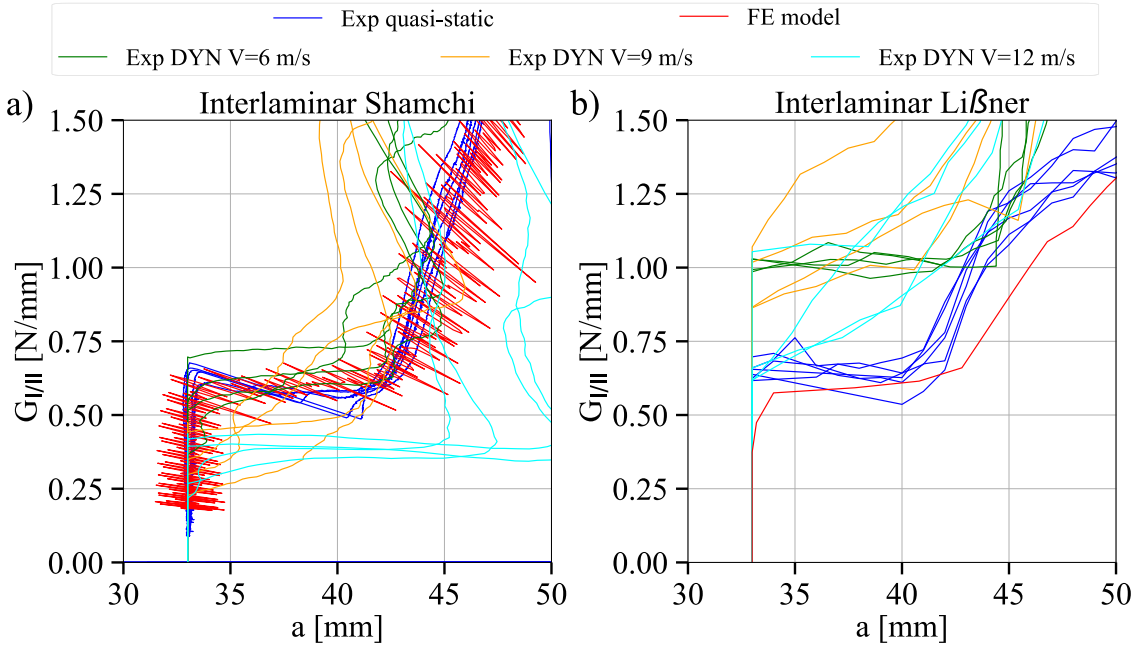

Fig. 19. Experimental R-curves for the SLB interlaminar specimens under different impact speeds. (a) With Shamchi et al. [5] and (b) with Lißner et al. [15] data reduction methods, respectively.

the mode II and mixed mode fracture toughness decreased with the impact speed, both for adhesive and interlaminar cases and thus, crack propagation onset occurred earlier. For example, for the adhesive joint, the mode II fracture toughness decreased from 2.4 N/mm (quasi-static) down to 0.89 N/mm for the largest speed considered, while this decrease for the interlaminar case was from 2.6 N/mm (quasi-static) down to 2.1 N/mm (dynamic). The effect was more important for the adhesive joint. Instead, the direct method by Lißner provided in general the opposite trend: the fracture toughness increased for mode II interlaminar and adhesive, and for interlaminar under mixed mode, therefore, crack propagation onset was delayed. Only for the adhesive case under mixed mode the results were more consistent between both data reduction methods. The authors attribute the difference between both methods to the large uncertainties in the measurement of the crack length during the dynamic tests, that is needed by Lißner approach. Consequently, the results provided by Shamchi method are assumed to be more reliable.

Future work will expand this study by developing new test methods for the dynamic mode II and mixed mode interlaminar characterisation. In addition, alternative methodologies to carry out the data reduction will be explored, for instance by instrumenting the specimen directly with strain gauges. More advanced numerical models, including strain rate effects, will also be developed with the objective of reproducing the experimental cases here shown, which could help to further understand the results presented in this paper.

CRediT authorship contribution statement

José M. Guerrero: Writing – review & editing, Writing – original draft, Validation, Methodology, Investigation, Formal analysis, Conceptualization. **Emilio V. González:** Writing – review & editing, Validation, Supervision, Project administration, Methodology, Investigation, Formal analysis, Conceptualization. **José A. Artero:** Writing – review & editing, Validation, Methodology, Investigation, Formal analysis, Conceptualization. **Adrián Cimadevilla:** Writing – review & editing, Validation, Methodology, Investigation, Formal analysis, Conceptualization. **J.M. Rodríguez-Sereno:** Writing – review & editing, Validation, Methodology, Investigation, Formal analysis, Conceptualization. **Joan A. Mayugo:** Writing – review & editing, Validation, Methodology, Investigation, Formal analysis, Conceptualization. **Elisabeth De Blanpre:** Writing – review & editing, Validation, Supervision, Methodology, Investigation, Formal analysis, Conceptualization. **Vincent Jacques:** Writing – review & editing, Validation, Supervision, Methodology, Investigation, Formal analysis, Conceptualization.

Declaration of competing interest

The authors declare that they have no known competing financial interests or personal relationships that could have appeared to influence the work reported in this paper.

Data availability

The authors do not have permission to share data.

Acknowledgements

This work was carried out under the framework of the EU H2020 Clean Sky 2 Project BEDYN - Development of a methodology (test, measurement, analysis) to characterise the BEhaviour of composite structures under DYNamic loading, developed within the consortium of AMADE research group from the University of Girona, the University of Carlos III of Madrid and the company COMPOXY, with Dassault Aviation being the project topic manager. This work has received funding from the Clean Sky 2 Joint Undertaking (JU) under grant agreement No. 886519. The JU receives support from the European Union's Horizon 2020 research and innovation programme and the Clean Sky 2 JU members other than the Union. José M. Guerrero would also like to acknowledge the funding of the post-doc grant Margarita Salas with reference REQ2021_A_15, financed by the Spanish 'Ministerio de Universidades' and the European Union - Next GenerationEU. Open Access funding provided thanks to the CRUE-CSIC agreement with Elsevier.

References

[1] Turon A, Costa J, Maimí P, Trias D, Mayugo J. A progressive damage model for unidirectional fibre-reinforced composites based on fibre fragmentation. Part I: Formulation. Compos Sci Technol 2005;65(13):2039–48. http://dx.doi.org/10.1016/j.compscitech.2005.04.012.

[2] González EV, Maimí P, Camanho PP, Turon A, Mayugo JA. Simulation of drop-weight impact and compression after impact tests on composite laminates. Compos Struct 2012;94(11):3364–78. http://dx.doi.org/10.1016/j.compstruct.2012.05.015.

[3] May M, Channammagari H, Hahn P. High-rate mode II fracture toughness testing of polymer matrix composites – A review. Composites A 2020;137(June):106019. http://dx.doi.org/10.1016/j.compositesa.2020.106019.

[4] Ramji A, Xu Y, Yasaee M, Grasso M, Webb P. Influence of veil interleave distribution on the delamination resistance of cross-ply CFRP laminates under low velocity impact. Int J Impact Eng 2021;157(August):103997. http://dx.doi.org/10.1016/j.ijimpeng.2021.103997.

[5] Shamchi SP, de Moura MF, Zhao Z, Yi X, Moreira PM. Dynamic mode II interlaminar fracture toughness of electrically modified carbon/epoxy composites. Int J Impact Eng 2022;159(September 2021):104030. http://dx.doi.org/10.1016/j.ijimpeng.2021.104030.

[6] Maimí P, Camanho PP, Mayugo JA, Dávila CG. A continuum damage model for composite laminates: Part II - Computational implementation and validation. Mech Mater 2007;39(10):909–19. http://dx.doi.org/10.1016/j.mechmat.2007.03.006.

[7] Camanho PP, Bessa MA, Catalanotti G, Vogler M, Rolfes R. Modeling the inelastic deformation and fracture of polymer composites-Part II: Smeared crack model. Mech Mater 2013;59:36–49. http://dx.doi.org/10.1016/j.mechmat.2012.12.001.

[8] Serra J, Bouvet C, Castanié B, Petiot C. Scaling effect in notched composites: The Discrete Ply Model approach. Compos Struct 2016;148:127–43. http://dx.doi.org/10.1016/j.compstruct.2016.03.062.

[9] Furtado C, Catalanotti G, Arteiro A, Gray PJ, Wardle BL, Camanho PP. Simulation of failure in laminated polymer composites: Building-block validation. Compos Struct 2019;226(June):111168. http://dx.doi.org/10.1016/j.compstruct.2019.111168.

[10] Cózar I, Otero F, Maimí P, González E, Miot S, Turon A, et al. A three-dimensional plastic-damage model for polymer composite materials. Composites A 2022;163(September):107198. http://dx.doi.org/10.1016/j.compositesa.2022.107198.

[11] Heimbs S, Heller S, Middendorf P, Hähnel F, Weiße J. Low velocity impact on CFRP plates with compressive preload: Test and modelling. Int J Impact Eng 2009;36(10–11):1182–93. http://dx.doi.org/10.1016/j.ijimpeng.2009.04.006.

[12] Cui H, Thomson D, Eskandari S, Petrinic N. A critical study on impact damage simulation of IM7/8552 composite laminate plate. Int J Impact Eng 2019;127(January):100–9. http://dx.doi.org/10.1016/j.ijimpeng.2019.01.009.

[13] Blackman BR, Kinloch AJ, Rodriguez Sanchez FS, Teo WS, Williams JG. The fracture behaviour of structural adhesives under high rates of testing. Eng Fract Mech 2009;76(18):2868–89. http://dx.doi.org/10.1016/j.engfracmech.2009.07.013.

[14] May M, Hesebeck O, Marzi S, Böhme W, Lienhard J, Kilchert S, et al. Rate dependent behavior of crash-optimized adhesives - Experimental characterization, model development, and simulation. Eng Fract Mech 2015;133:112–37. http://dx.doi.org/10.1016/j.engfracmech.2014.11.006.

[15] Lißner M, Alabort E, Erice B, Cui H, Blackman BRK, Petrinic N. On the dynamic response of adhesively bonded structures. Int J Impact Eng 2020;138(October 2019):103479. http://dx.doi.org/10.1016/j.ijimpeng.2019.103479.

[16] Daniel IM, Werner BT, Fenner JS. Strain-rate-dependent failure criteria for composites. Compos Sci Technol 2011;71(3):357–64. http://dx.doi.org/10.1016/j.compscitech.2010.11.028.

[17] May M, Lässig T. Rate-dependent mode I delamination in ballistic composites – Experiment and simulation. Compos Struct 2017;180:596–605. http://dx.doi.org/10.1016/j.compstruct.2017.08.045.

[18] Smiley AJ, Pipes RB. Rate sensitivity of mode II interlaminar fracture toughness in graphite/epoxy and graphite/PEEK composite materials. Compos Sci Technol 1987;29(1):1–15. http://dx.doi.org/10.1016/0266-3538(87)90033-9.

[19] Maikuma H, Gillespie JW, Wilkins DJ. Mode II interlaminar fracture of the center notch flexural specimen under impact loading. J Compos Mater 1990;24(2):124–49. http://dx.doi.org/10.1177/002199839002400201.

[20] Kageyama K, Kimpara I. Delamination failures in polymer composites. Mater Sci Eng A 1991;143(1–2):167–74. http://dx.doi.org/10.1016/0921-5093(91)90736-7.

[21] Blackman BR, Dear JP, Kinloch AJ, MacGillivray H, Wang Y, Williams JG, et al. The failure of fibre composites and adhesively bonded fibre composites under high rates of test: Part III mixed-mode I/II and mode II loadings. J Mater Sci 1996;31(17):4467–77. http://dx.doi.org/10.1007/BF00366342.

[22] Kusaka T, Hojo M, Ochiai S, Kurokawa T. Rate-dependent mode II interlaminar fracture behavior of carbon-fiber/epoxy composite laminates. Mater Sci Res Int 1999;5(2):98–103.

[23] Tsai JL, Guo C, Sun CT. Dynamic delamination fracture toughness in unidirectional polymeric composites. Compos Sci Technol 2001;61(1):87–94. http://dx.doi.org/10.1016/S0266-3538(00)00197-4.

[24] Nwosu SN, Hui D, Dutta PK. Dynamic mode II delamination fracture of unidirectional graphite/epoxy composites. Composites B 2003;34(3):303–16. http://dx.doi.org/10.1016/S1359-8368(02)00039-2.

[25] Yokoyama T. Experimental determination of impact tensile properties of adhesive butt joints with the split Hopkinson bar. J Strain Anal Eng Des 2003;38(3):233–45. http://dx.doi.org/10.1243/03093240376531056.

[26] Wu XF, Dzenis YA. Determination of dynamic delamination toughness of a graphite-fiber/epoxy composite using hopkinson pressure bar. Polym Compos 2005;26(2):165–80. http://dx.doi.org/10.1002/pc.20093.

[27] Raykhere SL, Kumar P, Singh RK, Parameswaran V. Dynamic shear strength of adhesive joints made of metallic and composite adherents. Mater Des 2010;31(4):2102–9. http://dx.doi.org/10.1016/j.matdes.2009.10.043.

[28] De Moura MF, Dourado N, Morais JJ, Pereira FA. Numerical analysis of the ENF and ELS tests applied to mode II fracture characterization of cortical bone tissue. Fatigue Fract Eng Mater Struct 2011;34(3):149–58. http://dx.doi.org/10.1111/j.1460-2695.2010.01502.x.

[29] Colin de Verdiere M, Skordos AA, Walton AC, May M. Influence of loading rate on the delamination response of untufted and tufted carbon epoxy non-crimp fabric composites/Mode II. Eng Fract Mech 2012;96:1–10. http://dx.doi.org/10.1016/j.engfracmech.2011.12.011.

[30] Yokoyama T, Nakai K. Determination of the impact tensile strength of structural adhesive butt joints with a modified split Hopkinson pressure bar. Int J Adhes Adhes 2015;56:13–23. http://dx.doi.org/10.1016/j.ijadhadh.2014.07.011.

[31] Wiegand J, Hornig A, Gerlach R, Neale C, Petrinic N, Hufenbach W. An experimental method for dynamic delamination analysis of composite materials by impact bending. Mech Adv Mater Struct 2015;22(5):413–21. http://dx.doi.org/10.1080/15376494.2012.736066.

[32] Neumayer J, Kuhn P, Koerber H, Hinterhölzl R. Experimental determination of the tensile and shear behaviour of adhesives under impact loading. J Adhes 2016;92(7–9):503–16. http://dx.doi.org/10.1080/00218464.2015.1092387.

[33] Yasaee M, Mohamed G, Pellegrino A, Petrinic N, Hallett SR. Strain rate dependence of mode II delamination resistance in through thickness reinforced laminated composites. Int J Impact Eng 2017;107:1–11. http://dx.doi.org/10.1016/j.ijimpeng.2017.05.003.

[34] Sassi S, Tarfaoui M, Benyahia H. Experimental study of the out-of-plane dynamic behaviour of adhesively bonded composite joints using split Hopkinson pressure bars. J Compos Mater 2018;52(21):2875–85. http://dx.doi.org/10.1177/0021998318758368.

[35] Machado JJ, Marques EA, da Silva LF. Adhesives and adhesive joints under impact loadings: An overview. J Adhes 2018;94(6):421–52. http://dx.doi.org/10.1080/00218464.2017.1282349.

[36] Lißner M, Alabort E, Cui H, Pellegrino A, Petrinic N. On the rate dependent behaviour of epoxy adhesive joints: Experimental characterisation and modelling of mode I failure. Compos Struct 2018;189(September 2017):286–303. http://dx.doi.org/10.1016/j.compstruct.2018.01.019.

[37] Isakov M, May M, Hahn P, Paul H, Nishi M. Fracture toughness measurement without force data – Application to high rate DCB on CFRP. Composites A 2019;119(January):176–87. http://dx.doi.org/10.1016/j.compositesa.2019.01.030.

[38] Medina SA, González EV, Blanco N, Pernas-Sánchez J, Artero-Guerrero JA. Guided Double Cantilever Beam test method for intermediate and high loading rates in composites. Int J Solids Struct 2023;264(June 2022):112118. http://dx.doi.org/10.1016/j.ijsolstr.2023.112118.

[39] Medina SA, González EV, Blanco N, Maimí P, Pernas-Sánchez J, Artero-Guerrero JA, et al. Rate-dependency analysis of mode I delamination by means of different data reduction strategies for the GDCB test method. Eng Fract Mech 2023;288(May). http://dx.doi.org/10.1016/j.engfracmech.2023.109352.

[40] Cantwell WJ. The influence of loading rate on the mode II interlaminar fracture toughness of composite materials. J Compos Mater 1997;31(14):1364–80. http://dx.doi.org/10.1177/002199839703101401.

[41] ASTM D6671 / D6671M-22. Standard test method for mixed mode I-mode II interlaminar fracture toughness of unidirectional fiber reinforced polymer matrix composites. West Conshohocken, PA: ASTM International; 2019, URL https://www.astm.org/d7905_d7905m-19e01.html.

[42] Dassault Systemes/ SIMULIA. ABAQUS, Inc. ABAQUS version 2022 Documentation. 2022.

[43] ASTM D3039 / D3039M-17. Standard test method for tensile properties of polymer matrix composite materials. West Conshohocken, PA: ASTM International; 2017, URL https://www.astm.org/d3039_d3039m-17.html.

[44] ASTM D6641 / D6641M. Standard test method for compressive properties of polymer matrix composite materials using a combined loading compression (CLC) test fixture. West Conshohocken, PA: ASTM International; 2021, URL https://www.astm.org/d6641_d6641m-16e02.html.

[45] ASTM D3518 / D3518M-18. Standard test method for in-plane shear response of polymer matrix composite materials by tensile test of a ±45° laminate. West Conshohocken, PA: ASTM International; 2018, URL https://www.astm.org/d3518_d3518m-18.html.

[46] Benzeggagh ML, Kenane M. Measurement of mixed-mode delamination fracture toughness of unidirectional glass/epoxy composites with mixed-mode bending apparatus. Compos Sci Technol 1996;56:439–49. http://dx.doi.org/10.1016/0266-3538(96)00005-X.

[47] ISO 25217:2009. Adhesives – Determination of the mode 1 adhesive fracture energy of structural adhesive joints using double cantilever beam and tapered double cantilever beam specimens. ISO; 2020, URL https://www.iso.org/standard/42797.html.

[48] ISO 15024:2001. Fibre-reinforced plastic composites — Determination of mode I interlaminar fracture toughness, GIC, for unidirectionally reinforced materials. ISO; 2023, URL https://www.iso.org/standard/25581.html.

[49] ASTM D6671 / D6671M-22. Standard test method for mixed mode I-mode II interlaminar fracture toughness of unidirectional fiber reinforced polymer matrix composites. West Conshohocken, PA: ASTM International; 2022, URL https://www.astm.org/d6671_d6671m-22.html.

[50] ISO 15114:2014. Fibre-reinforced plastic composites – Determination of the mode II fracture resistance for unidirectionally reinforced materials using the calibrated end-loaded split (C-ELS) test and an effective crack length approach. ISO; 2019, URL https://www.iso.org/standard/55357.html.

[51] Soto A, González EV, Maimí P, Turon A, Sainz de Aja JR, de la Escalera FM. Cohesive zone length of orthotropic materials undergoing delamination. Eng Fract Mech 2016;159:174–88. http://dx.doi.org/10.1016/j.engfracmech.2016.03.033.

[52] Guerrero JM, Sasikumar A, Llobet J, Costa J. Experimental and virtual testing of a composite-aluminium aircraft wingbox under thermal loading. Aerosp Sci Technol 2023;138:108329. http://dx.doi.org/10.1016/j.ast.2023.108329.